Part B

Development of gauges for interacting Bose gases

Chapter 7

Gauges for single-mode interacting Bose gas dynamics

7.1 Motivation

Simulations of the dynamics of multi-mode (locally) interacting Bose gases (with lattice Hamiltonian (2.17)) using the positive P representation suffer two major technical problems caused by instabilities in the stochastic equations: 1) Exponential growth of distribution broadness leading to rapid loss of any useful accuracy. 2) Probable moving singularities when two or more modes are coupled (See Section 7.2.5). These issues prevent simulation of all but short time behaviour. Gases with non-local interactions (Hamiltonian (2.12)) are expected to suffer from similar problems on the basis that the locally-interacting lattice model is a special case of these more general models.

The instabilities arise from the two-body interaction terms in the Hamiltonian, and so for a locally-interacting model the unstable processes decouple and are local to each spatial lattice mode of the model. Hence, if the instabilities are brought under control for each mode on its own, then simulations of the full many-mode model should benefit as well.

In this chapter, a single-boson mode with two-body interactions is considered, and gauges (kernel drift and diffusion) are introduced to make improvements. A

drift gauge can remove the offending instability, while the diffusion gauge makes a tradeoff between noise in the phase-space (i.e. α and β) equations and noise in the global weight z_0, and will be optimized to improve simulation times. In Chapter 8, the performance of the method developed here will be investigated in a coupled two-mode system as a prelude to multi-mode simulations.

7.2 The single-mode interacting Bose gas

7.2.1 Physical model

Consider a single mode extracted from the open multi-mode locally-interacting lattice model of Section 2.5. Annihilation and creation operators for the mode are $\widehat{a}$ and $\widehat{a}^\dagger$, and obey $[\widehat{a}, \widehat{a}^\dagger] = 1$. From (2.17), and with possible coherent gain added as in (2.25), the Hamiltonian is

$$\widehat{H} = \hbar\widehat{n}\left(\omega + \chi\left[\widehat{n} - 1\right]\right) + i\hbar(\varepsilon\widehat{a}^\dagger - \varepsilon^*\widehat{a}), \tag{7.1}$$

The master equation of this system interacting with an environment is given by the usual Linblad form (2.20), with Linblad operators

$$\widehat{L}_1 = \widehat{a}\sqrt{\gamma(1+\overline{n}_{\rm bath})} \tag{7.2a}$$

$$\widehat{L}_2 = \widehat{a}^\dagger\sqrt{\gamma\overline{n}_{\rm bath}} \tag{7.2b}$$

modeling single-particle interactions with a standard boson heat bath with a mean number of particles $\overline{n}_{\rm bath}(T)$ per bath mode, as in Section 2.5.

Physically this model approximates a single mode of interest $\mathbf{n}$ of a multi-mode system with two-body scattering, where evolution of the other modes $\mathbf{m} \neq \mathbf{n}$ is assumed negligible. Roughly, the linear self-energy term becomes $\omega = \omega_{\mathbf{nn}}$, highly occupied coherent modes $\mathbf{m}$ can be collected into $\varepsilon = -i\sum_{\mathbf{m}}\omega_{\mathbf{nm}}\langle\widehat{a}_{\mathbf{m}}\rangle$, while the remainder of modes can become the heat bath. The single-mode model can also sometimes represent an approximation to a single orbital of a more complex system, if the constants ω,ε, $\overline{n}_{\rm bath}$ and χ are chosen appropriately.

7.2.2 Stochastic gauge P equations

A single-mode gauge P kernel (6.33) is used, where the complex configuration variables are coherent state amplitudes α and β, and a global weight $\Omega = e^{z_0}$. From the multi-mode equations (5.17), (5.18), and (5.21) of Section 5.3, the gauge P Ito equations for this model are

$$d\alpha = -i\omega\alpha\,dt - 2i\chi\alpha^2\beta\,dt - \frac{\gamma}{2}\alpha\,dt + \epsilon\,dt + \sum_k \underline{B}_{1k}(dW_k - \mathcal{G}_k\,dt) \quad (7.3a)$$

$$d\beta = i\omega\beta\,dt + 2i\chi\beta^2\alpha\,dt - \frac{\gamma}{2}\beta\,dt + \epsilon^*\,dt + \sum_k \underline{B}_{2k}(dW_k - \mathcal{G}_k\,dt) \quad (7.3b)$$

$$d\Omega = \Omega\sum_k \mathcal{G}_k dW_k, \quad (7.3c)$$

where the pre-drift-gauge noise matrices $\underline{B}_{jk}$ defined as in Section 4.3.1 and drift gauges $\mathcal{G}_k$ have not been specified yet. The dW_k are independent Wiener increments, which can be implemented by Gaussian noises of variance dt. The elements of the $2 \times N_W$ complex noise matrices $\underline{B}$ satisfy

$$\underline{D}_{11} = \sum_k \underline{B}_{1k}^2 = -2i\chi\alpha^2 \quad (7.4a)$$

$$\underline{D}_{22} = \sum_k \underline{B}_{2k}^2 = 2i\chi\beta^2 \quad (7.4b)$$

$$\underline{D}_{12} = \sum_k \underline{B}_{1k}\underline{B}_{2k} = \gamma\overline{n}_{\rm bath}(T). \quad (7.4c)$$

The N_W complex drift gauge functions $\mathcal{G}_k$ are arbitrary in principle.

The standard gauge formulation (4.90) will be used, with the proviso that noises related to the bath interaction and the interparticle interactions are chosen to be independent to simplify the equations as outlined in Section 4.4.7. That is, using diffusion matrix $\underline{D} = \underline{B}\,\underline{B}^T = \sum_l \underline{D}^{(l)}$ with

$$\underline{D}^{(1)} = 2i\chi\begin{bmatrix} -\alpha^2 & 0 \\ 0 & \beta^2 \end{bmatrix} \quad ; \quad \underline{D}^{(2)} = \gamma\overline{n}_{\rm bath}(T)\begin{bmatrix} 0 & 1 \\ 1 & 0 \end{bmatrix}, \quad (7.5)$$

one obtains the square root noise matrix forms

$$\underline{B}_0^{(1)} = \sqrt{2i\chi}\begin{bmatrix} i\alpha & 0 \\ 0 & \beta \end{bmatrix} \quad ; \quad \underline{B}_0^{(2)} = \sqrt{\frac{\gamma\overline{n}_{\rm bath}(T)}{2}}\begin{bmatrix} 1 & i \\ 1 & -i \end{bmatrix}. \quad (7.6)$$

In Section 7.2.4 it will be shown that the process responsible for instabilities is the two-particle collisions (parameterized by χ), and so improvements should be

searched for by gauging this process, not the bath interactions (parameterized by γ). Thus, the standard gauges are applied as:

1. Imaginary diffusion gauges g''_{jk} as in Section 4.5. Recall from Sections 4.4.3 and 4.4.4 that only imaginary standard diffusion gauges can alter the stochastic behaviour of the simulation, so only these will be considered. One obtains

$$\underline{B} = \left[\begin{array}{cc} \underline{B}_0^{(1)} O(g''_{12}) & \underline{B}_0^{(2)} \end{array} \right], \tag{7.7}$$

   with an orthogonal matrix O of the form (4.68) dependent on a single imaginary diffusion gauge $g_{12} = ig''$ with real g''.

2. Complex drift gauges $\mathcal{G}_1$ and $\mathcal{G}_2$, with the remaining $\mathcal{G}_{k>2} = 0$.

The two-variable diagonal diffusion gauge expression (4.71) applies here, and the Ito stochastic equations become

$$\begin{aligned} d\alpha &= -i\omega\alpha\,dt - 2i\chi\alpha^2\beta\,dt - \frac{\gamma}{2}\alpha\,dt + \epsilon\,dt + \sqrt{\gamma\overline{n}_{\rm bath}}d\eta_{\rm bath} \\ &\quad + i\alpha\sqrt{2i\chi}\left[(dW_1 - \mathcal{G}_1\,dt)\cosh g'' + i(dW_2 - \mathcal{G}_2\,dt)\sinh g''\right] \qquad (7.8a) \\ d\beta &= i\omega\beta\,dt + 2i\chi\beta^2\alpha\,dt - \frac{\gamma}{2}\beta\,dt + \epsilon^*\,dt + \sqrt{\gamma\overline{n}_{\rm bath}}d\eta^*_{\rm bath} \\ &\quad + \beta\sqrt{2i\chi}\left[-i(dW_1 - \mathcal{G}_1\,dt)\sinh g'' + (dW_2 - \mathcal{G}_2\,dt)\cosh g''\right] \qquad (7.8b) \\ d\Omega &= \Omega\left\{\mathcal{G}_1 dW_1 + \mathcal{G}_2 dW_2\right\} \qquad (7.8c) \end{aligned}$$

in terms of the real Wiener increments dW_1, dW_2 implemented by Gaussian noises of variance dt, and the complex stochastic Wiener-like increment $d\eta_{\rm bath}$ obeying $\langle d\eta_{\rm bath} d\eta^*_{\rm bath}\rangle_{\rm stoch} = dt$ and $\langle d\eta^2_{\rm bath}\rangle_{\rm stoch} = 0$.

7.2.3 Anharmonic oscillator

Consider the gain-less system ($\overline{n}_{\rm bath}(T) = \varepsilon = 0$), which contains all the essential features of the two-body interactions. This system is known in the literature as the damped anharmonic oscillator.

For this toy system, the observables can be solved analytically, and comparing simulations with these will be of great use here to optimize diffusion gauge choices. In particular, consider coherent state projector initial conditions $|\alpha_0\rangle\langle\beta_0^*|$, which

correspond to the configuration of a single trajectory out of the $\mathcal{S}$ system samples that together can represent any arbitrary quantum state. Let us concentrate on the mean particle number

$$\langle \widehat{n} \rangle = \langle \widehat{a}^\dagger \widehat{a} \rangle, \tag{7.9}$$

and the first-order time correlation function[1]

$$G^{(1)}(0,t) = \beta_0 \langle \widehat{a} \rangle = \alpha_0^* \langle \widehat{a}^\dagger \rangle^*, \tag{7.10}$$

which contains phase coherence information. Normalizing by $\langle \alpha_0 | \beta_0^* \rangle = \mathrm{Tr}\left[\, |\alpha_0\rangle \langle \beta_0^*| \,\right]$, their expectation values are found to be

$$\langle \widehat{n} \rangle = n_0 \, e^{-\gamma t}, \tag{7.11a}$$

$$G^{(1)}(0,t) = n_0 \, e^{-\gamma t/2} \, e^{-i\omega t} \exp\left\{ \frac{n_0}{1 - i\gamma/2\chi} \left(e^{-2i\chi t - \gamma t} - 1 \right) \right\}, \tag{7.11b}$$

where $n_0 = \alpha_0 \beta_0$.

When the damping is negligible, n_0 real, and the number of particles is $n_0 \gg 1$, one sees that the initial phase oscillation period (ignoring ω) is

$$t_{\mathrm{osc}} = \frac{1}{2\chi} \sin^{-1}\left(\frac{2\pi}{n_0} \right) \approx \frac{\pi}{\chi n_0}, \tag{7.12}$$

and the phase coherence time, over which $|G^{(1)}(0,t)|$ decays is

$$t_{\mathrm{coh}} = \frac{1}{2\chi} \cos^{-1}\left(1 - \frac{1}{2n_0} \right) \approx \frac{1}{2\chi\sqrt{n_0}}. \tag{7.13}$$

The first quantum revival occurs at

$$t_{\mathrm{revival}} = \frac{\pi}{\chi}. \tag{7.14}$$

[1]This first order correlation function is usually written in the Heisenberg picture as $G^{(1)}(0,t) = \langle \widehat{a}^\dagger(0) \widehat{a}(t) \rangle$. Moving to the Schrödinger picture in which the gauge P representation is defined, one has $G^{(1)} = \mathrm{Tr}\left[e^{i\widehat{H}t/\hbar} \widehat{a} e^{-i\widehat{H}t/\hbar} \widehat{\rho}(0) \widehat{a}^\dagger \right]$. Because of the coherent state conditions used here, $\widehat{\rho}(0) = \widehat{\Lambda}(\alpha_0, \beta_0, \Omega = 1)$. Thus, $\widehat{\rho}(0)\widehat{a}^\dagger = \beta_0 \widehat{\rho}(0)$ using (5.7d). This gives $G^{(1)} = \beta_0 \mathrm{Tr}\left[\widehat{a} e^{-i\widehat{H}t/\hbar} \widehat{\rho}(0) \, e^{i\widehat{H}t/\hbar} \right]$, and identifying the Schrödinger picture density matrix as $\widehat{\rho}(t) = e^{-i\widehat{H}t/\hbar} \widehat{\rho}(0) \, e^{i\widehat{H}t/\hbar}$, this gives the desired expression $G^{(1)}(0,t) = \beta_0 \langle \widehat{a} \rangle$. To obtain the right-hand side expression in (7.10), note that $G^{(1)}$ is a complex quantity composed of two observables (see (7.20)) — one for the real, and one for the imaginary part. Taking the adjoint, $G^{(1)}(0,t)^* = \langle \widehat{a}^\dagger(t) \widehat{a}(0) \rangle$ in the Heisenberg picture, and following the same procedure as above, one obtains $G^{(1)}(0,t)^* = \alpha_0 \langle \widehat{a}^\dagger \rangle$.

The stochastic equations for this gain-less system are more convenient in terms of the logarithmic number-phase variables

$$n_L = \log(\alpha\beta) \tag{7.15a}$$

$$m_L = \log\left(\frac{\alpha}{\beta}\right). \tag{7.15b}$$

For coherent states where $\beta = \alpha^*$, n_L is the logarithm of the mean number of particles $|\alpha|^2$, while $m_L = 2i\angle\alpha$, and characterizes the phase of the coherent amplitude. The Ito equations in the new variables are

$$dn_L = -\gamma\, dt + 2i\sqrt{i\chi}e^{-g''}(d\eta - \mathcal{G}_{(n)}\, dt) \tag{7.16a}$$

$$dm_L = -2i(\omega - \chi + 2\chi e^{n_L})\, dt + 2i\sqrt{i\chi}e^{g''}(d\eta^* - \mathcal{G}_{(m)}\, dt) \tag{7.16b}$$

$$dz_0 = \mathcal{G}_{(m)}d\eta + \mathcal{G}_{(n)}d\eta^* - \mathcal{G}_{(n)}\mathcal{G}_{(m)}\, dt = d(\log\Omega), \tag{7.16c}$$

where the complex Wiener-like increment $d\eta = (dW_1 - idW_2)/\sqrt{2}$ has variances

$$\langle d\eta d\eta^*\rangle_{\text{stoch}} = dt \tag{7.17a}$$

$$\left\langle d\eta^2\right\rangle_{\text{stoch}} = 0, \tag{7.17b}$$

and the independent transformed complex drift gauge functions are

$$\mathcal{G}_{(n)} = \frac{\mathcal{G}_1 - i\mathcal{G}_2}{\sqrt{2}} \quad ; \quad \mathcal{G}_{(m)} = \frac{\mathcal{G}_1 + i\mathcal{G}_2}{\sqrt{2}}. \tag{7.18a}$$

Note: these are not necessarily complex conjugates since the original $\mathcal{G}_1$ and $\mathcal{G}_2$ are in general complex.

7.2.4 Behaviour of the positive P simulation

Lack of moving singularities

Consider the anharmonic oscillator equations (7.16) in the positive P representation, where $\mathcal{G}_k = 0$, and $g'' = 0$. By comparison with the condition (6.3), one can check by inspection that moving singularities do not occur : dn_L does not depend on any variables and so is stable, while dm_L depends only on the other variable n_L. Thus the deterministic behaviour of m_L is just integration of a finite function of n_L (which itself remains finite). The noise in m_L is of constant magnitude. z_0 does

not evolve. All variables remain finite, no moving singularities or noise divergences occur. Therefore, none of the symptoms of boundary term errors from Section 6.1.2 are present in the equations.

Indeed, the investigations of Gilchrist *et al*[64] found that boundary term errors do not occur for the special case of the single-mode anharmonic oscillator.

Rapid growth of statistical error

If the observable estimators converge to the quantum mechanical expectation values in the limit of many trajectories so that *accuracy* of the simulation is not a problem, there still remains the issue of how large a sample of trajectories has to be to give a *precise* result.

While the evolution of n_L is well-behaved, being simply constant isotropic diffusion and possibly some decay, the deterministic evolution of m_L can be very sensitive to n_L due to the exponential drift term.

Particularly $\mathrm{Re}\{m_L\}$ has a great influence on observable estimates of phase-dependent observables, such as $G^{(1)}(0,t)$. Consider the quadrature observables

$$\widehat{q}(\theta) = \frac{\widehat{a}e^{i\theta} + \widehat{a}^\dagger e^{-i\theta}}{2}, \tag{7.19}$$

which are closely related to the first-order correlation function

$$G(0,t) = \beta_0\langle\widehat{q}(0) - i\widehat{q}(\pi/2)\rangle = (\alpha_0\langle\widehat{q}(0) + i\widehat{q}(\pi/2)\rangle)^* . \tag{7.20}$$

Comparing to (5.10) and (5.13), the estimator for $\langle\widehat{q}\rangle$ is

$$\overline{q}(\theta) = \frac{\left\langle \mathrm{Re}\left\{\frac{\Omega}{2}\left(\alpha e^{i\theta} + \beta e^{-i\theta}\right)\right\}\right\rangle_{\mathrm{stoch}}}{\left\langle \mathrm{Re}\left\{\Omega\right\}\right\rangle_{\mathrm{stoch}}} \tag{7.21}$$

$$= \frac{\left\langle \mathrm{Re}\left\{\exp\left(z_0 + \frac{n_L}{2}\right)\cosh\left(i\theta + \frac{m_L}{2}\right)\right\}\right\rangle_{\mathrm{stoch}}}{\left\langle \mathrm{Re}\left\{e^{z_0}\right\}\right\rangle_{\mathrm{stoch}}}. \tag{7.22}$$

We can see that $\overline{q}$ is very sensitive to $\mathrm{Re}\{m_L\}$ due to the cosh factor. This real part of m_L evolves as

$$d\mathrm{Re}\{m_L\} = 4\chi e^{\mathrm{Re}\{n_L\}}\sin(\mathrm{Im}\{n_L\})\,dt + \ldots, \tag{7.23}$$

which can be a very rapid growth even for moderate values of $\mathrm{Re}\{n_L\}$. Worse, even a moderate spread in $\mathrm{Re}\{n_L\}$ leads rapidly to a very wide *spread* of $\mathrm{Re}\{m_L\}$,

not to mention the spread in the factor $\cosh(m_L/2)$ that appears in the observable estimate. The behaviour of this spread will be considered in detail in Section 7.5.3, but for now it suffices to point out that there arises a characteristic time scale $t_{\rm sim}$ beyond which the uncertainty in phase-dependent observable estimates grows faster than exponentially with time, and any simulations become effectively useless no matter how many trajectories are calculated.

Numerical investigations (See Figure 7.3 and Table 7.1) found that a positive P simulation lasts at most for times

$$t_{\rm sim} \approx \frac{(1.27 \pm 0.08)}{\chi n_0^{2/3}}. \tag{7.24}$$

For large mode occupation $n_0 \gg 1$, this is not enough time for significant phase decoherence to occur (compare to $t_{\rm coh}$ in (7.13)). This unfavorable scaling is known to be a major unresolved stumbling block for positive P simulations of the interacting Bose gas model (2.1) in many physical regimes. For example, evaporative cooling simulations encounter such sampling problems upon the onset of Bose condensation[15]. The expression (7.24) indicates that the simulation time for a many-mode system is likely to be limited by the simulation time of the most highly occupied mode (this is confirmed by the simulations in Chapter 10), which makes it especially worthwile to improve simulation times at large mode occupations.

Greater stability when damped

Consider the evolution of the log-occupation n_L in (7.16). In a positive P simulation (with $g'' = 0$), the noise term produces a spread in both the real and imaginary parts of n_L of standard deviation $\sigma = \sqrt{2\chi t}$. To a good approximation, all trajectories in a reasonable-sized sample will lie within about 4σ of the mean value (which is $\log(n_0) - \gamma t$). If the values of $\mathrm{Re}\{n_L\}$ for all trajectories are $\ll -\log 2\chi$, then the nonlinear term in the dm_L evolution equation becomes negligible, and stability problems abate. This will occur if the damping γ is large enough in comparison with the two-particle collisions χ. In Section 7.5.4, this behaviour will be found to depend on the "damping strength" parameter (7.70), which will quantify what is meant by "γ big enough". The increased stability at higher damping is a well-known

feature of positive P simulations of the anharmonic oscillator, and/or an interacting Bose gas[46].

7.2.5 Coupling to other modes and moving singularities

Non phase-dependent observables such as $\widehat{n} = \widehat{a}^{\dagger}\widehat{a}$ can still be calculated at long times for the anharmonic oscillator with the positive P method, because the evolution of their estimators (e.g. $\langle e^{n_L}\rangle_{\text{stoch}}$) does not depend on the unstable m_L. This is no consolation, however, because we are *ultimately* interested in simulating many-mode systems. (Singe-mode toy problems will fall even to a brute force truncated number-state basis calculation, so all these involved stochastic schemes are only ultimately justified for many-mode models). When many modes are present, the convenient separation of n_L and m_L evolution seen in (7.16) is no longer present due to mode-mixing terms (from kinetics and external potentials). This occurs even for a single-mode model with nonzero pumping ε, or a finite-temperature heat bath $\overline{n}_{\text{bath}} > 0$, which also model underlying mode-coupling processes. If the n_L and m_L equations are coupled, the growth of the spread of $\text{Re}\,\{m_L\}$ will also feed the growth of the spread of n_L, making *all* moment calculations intractable after some relatively short time.

Furthermore, moving singularities may appear. Reverting back to considering the α and β equations (7.8), the Ito positive P evolution of α will be of the form

$$d\alpha = -2i\chi\alpha^2\beta\,dt + \epsilon\,dt + \ldots, \tag{7.25}$$

and in particular

$$d|\alpha| = 2\chi|\alpha|^2|\beta|\sin(\angle\alpha + \angle\beta)\,dt + \ldots. \tag{7.26}$$

When $|\beta|\sin(\angle\alpha + \angle\beta)$ is positive, this violates the no-moving-singularities conditions (6.3), $|\alpha|$ grows faster then exponentially, and moving singularities may be possible, leading to boundary term errors. This did not occur for the closed anharmonic oscillator only because of its special symmetry properties that allowed the convenient decoupled logarithmic form of the equations (7.16).

Thus it can be seen that when mode mixing occurs, there are two potential problems that can arise after short times:

1. Rapid appearance of massive statistical errors, masking observable estimates in noise.

2. Possible systematic biases caused by moving singularities in the equations.

Ways to deal with these issues will be investigated in this chapter for a single-mode system, and for coupled-mode systems in Chapter 8.

7.3 Drift gauges: Removal of instability

As was seen in (7.26), the instabilities in the equations arise from the nonlinear two-body drift terms, and in particular from the part that leads to super exponential growth of $|\alpha|$ or $|\beta|$. Defining the real and imaginary parts of the number variable

$$\breve{n} = \alpha\beta = e^{n_L} = n' + in'' \tag{7.27}$$

for convenience, the offending terms are:

$$d\alpha = 2\chi\alpha n'' \, dt + \ldots \tag{7.28a}$$

$$d\beta = -2\chi\beta n'' \, dt + \ldots \tag{7.28b}$$

whereas the terms

$$d\alpha = -2i\chi\alpha n' \, dt + \ldots \tag{7.29a}$$

$$d\beta = 2i\chi\beta n' \, dt + \ldots \tag{7.29b}$$

affect only the phase of α or β, and are harmless. Furthermore we can see that any nonzero value of $n'' = |\alpha|\mathrm{Im}\left\{\beta e^{i\angle\alpha}\right\}$ can lead to moving singularities (in α evolution if $n'' > 0$, or in β evolution if $n'' < 0$). Note that nonzero n'' are characteristic of "non-classical" states that cannot be represented by non-singular Glauber P distributions — i.e. as a mixture of coherent states. This is because for all coherent state trajectories $\beta = \alpha^*$, and so $\breve{n} = n'$ only.

Let us follow the heuristic procedure of Section 6.3.2 to remove the instabilities. Considering the points there, in order:

1. REMOVE INSTABILITY: Drift gauges $\mathcal{G}_k$ are chosen so that the terms causing the instability (7.28) are canceled by the drift correction. Assuming no other changes to the drift takes place, then from (7.8), after some algebra, one obtains the required gauges:

$$\mathcal{G}_1 = -\sqrt{2i\chi}\, n'' e^{-g''} \tag{7.30a}$$

$$\mathcal{G}_2 = i\sqrt{2i\chi}\, n'' e^{-g''} = -i\mathcal{G}_1 \tag{7.30b}$$

These effectively cause the replacement in the stochastic equations

$$-2i\chi\alpha\breve{n}\, dt \rightarrow -2i\chi\alpha n'\, dt \tag{7.31a}$$

$$2i\chi\beta\breve{n}\, dt \rightarrow 2i\chi\beta n'\, dt. \tag{7.31b}$$

In terms of the logarithmic variables, the scaled gauges (7.18) are

$$\mathcal{G}_{(n)} = 0 \tag{7.32a}$$

$$\mathcal{G}_{(m)} = -2\sqrt{i\chi}\, n'' e^{-g''} = \mathcal{G}_1\sqrt{2}. \tag{7.32b}$$

For the anharmonic oscillator, dn_L is unchanged from the positive P simulation, and the full equations are

$$dn_L = -\gamma\, dt + 2i\sqrt{i\chi}e^{-g''}d\eta \tag{7.33a}$$

$$dm_L = -2i(\omega - \chi + 2\chi \mathrm{Re}\,\{e^{n_L}\})\, dt + 2i\sqrt{i\chi}e^{g''}d\eta^* \tag{7.33b}$$

$$dz_0 = -2\sqrt{i\chi}\,\mathrm{Im}\,\{e^{n_L}\}\, e^{-g''}\, d\eta. \tag{7.33c}$$

2. CHECK AGAIN FOR MOVING SINGULARITIES: (Ignoring, for the time being, any dependence on g'' since the diffusion gauge has not been chosen yet)

   - Comparing to conditions (6.3), it is seen that the linear drift terms in parameters ε, ω, γ, and $\overline{n}_{\mathrm{bath}}$ in (7.8) will not lead to moving singularities.
   - The new nonlinear drift terms (7.31) have lost their radial component due to the drift gauges, and so do not lead to any moving singularities either.

- From (B.7), the Stratonovich corrections for $d\alpha$ and $d\beta$ are $i\chi\alpha\,dt$ and $-i\chi\beta\,dt$, respectively. These extra terms satisfy (6.3), and so do not contribute any moving singularities in any of the Ito-Stratonovich hybrid family of algorithms.
- That leaves the new dz_0 evolution. The weight deterministically tracks the n_L evolution, and from (7.33)

$$dz_0 \;=\; i\,\mathrm{Im}\,\{e^{n_L}\}\,(dn_L + \gamma\,dt), \tag{7.34}$$

  and so if $n_L = \log(\alpha\beta)$ remains finite for all trajectories (as is seen from the lack of moving singularities in α and β evolution), then so will z_0.

Thus it is seen that no new moving singularities are introduced provided g'' is well-enough behaved. The dependence on g'' is considered in Section 7.5.7.

3. The noise terms in $d\alpha$ and $d\beta$ are exponential in α, and so also satisfy (6.3) together with the noise terms of dz_0. thus noise divergences are absent, given a well behaved g''.

4. As desired, there are no discontinuities in equations, by inspection (provided g'' is well behaved).

5. Gauge efficiency. Comparing to corresponding sub-points from Section 6.3.2:

   (a) Corrections to the drift are necessary in all of phase space apart from the subspaces $n'' = 0$ of measure zero, so generally $\mathcal{G}_k \neq 0$ apart from this special region.

   (b) For general purpose calculations, one wishes to minimize the quantity $\sum_k |\mathcal{G}_k|^2$, given that the instabilities are removed. This is achieved by the gauges (7.30) as they are only just large enough to remove the instabilities, and do not introduce any other modifications to the $d\alpha$, or $d\beta$ equations.

   (c) Attractors? For the single-mode anharmonic oscillator when $\varepsilon = 0$, there are deterministic attractors in the phase space at vacuum ($n = 0$), and

$n = (\chi - \omega)/2\chi$ (Stratonovich) or $n = -\omega/2\chi$ (Ito). At all these, $n'' = 0$, so the gauge is also zero. This is the desired situation.

In the more complicated case of nonzero ε, there will be some stationary points elsewhere in phase space. One could try to construct some gauges that would behave as (7.30) in the far tails of phase space i.e. as $|\alpha|, |\beta| \to \infty$, but would be zero at these stationary points. In the broad picture, however, there seems little point to do this for the single-mode case, because in a many-mode simulation all modes will be coupled together by the kinetic interaction $\omega_{\mathbf{n}\neq\mathbf{m}}$, and ε will be different or absent.

(d) Rather than tailoring the simulation for a single observable $\widehat{O}$, the quantity $\sum_k |\mathcal{G}_k|^2$ was minimized here to keep the gauge applicable for a general case.

6. None of the features to be avoided occur.

   (a) The gauge is nonzero over a wide range of phase-space, including regions often visited.

   (b) The gauge does not change in a particularly rapid fashion in phase-space

   (c) The gauge is autonomous.

   (d) The drift gauges break the analyticity of the equations, as suggested by the conjecture of Section 6.1.4.

7.4 Exponentials of Gaussian random variables

From the single-mode equations for the locally-interacting Bose gas (7.8) (or indeed from the many-mode equations (5.17) or (5.50)), it is seen that noise terms due to the interparticle interactions are generally of the multiplicative form

$$d\alpha \propto \alpha\sqrt{\chi}\, dW_k + \ldots \qquad ; \qquad d\beta \propto \beta\sqrt{\chi}\, dW_k + \ldots . \tag{7.35}$$

This leads to Brownian-like motion in the *logarithmic* variables n_L or m_L, as e.g. in (7.16). On the other hand, the observable estimates (e.g. $\langle\widehat{n}\rangle$ or $G^{(1)}(0,t)$) typically

involve quantities such as α or $\alpha\beta$ — in the original non-logarithmic variables. Clearly there will be a lot of averaging over random variables that are of similar form to the exponential of a Gaussian. Let us investigate the behaviour of such random variables.

Let ξ be a Gaussian random variable of mean zero and variance unity, thus its distribution is

$$\Pr(\xi) = \frac{1}{\sqrt{2\pi}} \exp\left(-\frac{\xi^2}{2}\right). \tag{7.36}$$

The moments of ξ can be found by integration of (7.36) to be

$$\left\langle \xi^k \right\rangle_{\text{stoch}} = \begin{cases} \dfrac{k!}{2^{k/2}(k/2)!} & \text{if } k > 0 \text{ is even} \\ 0 & \text{if } k > 0 \text{ is odd} \end{cases} \tag{7.37}$$

Now let us define the exponential random variable

$$v_\sigma = v_0 e^{\sigma\xi} = e^{v_L} \tag{7.38}$$

with positive real σ and v_0. Using (7.37), the exponential variable's mean is

$$\langle v_\sigma \rangle_{\text{stoch}} = \overline{v}_\sigma = \sum_{k=0}^{\infty} \frac{\sigma^k \left\langle \xi^k \right\rangle_{\text{stoch}}}{k!} = v_0 \exp\left(\frac{\sigma^2}{2}\right). \tag{7.39}$$

and so, also

$$\text{var}\left[v_\sigma\right] = \sigma_v^2 = v_0^2 e^{\sigma^2}\left(e^{\sigma^2} - 1\right) = \left[\overline{v}_\sigma \sqrt{\left(\frac{\overline{v}_\sigma}{v_0}\right)^2 - 1}\right]^2. \tag{7.40}$$

If one is interested in estimating quantities such as $\overline{v}_\sigma$ using $\mathcal{S}$ samples, then by the Central Limit Theorem, the relative uncertainty in such a finite-sample estimate will be

$$\Delta\overline{v}_\sigma = \frac{\sigma_v}{\overline{v}_\sigma \sqrt{\mathcal{S}}}. \tag{7.41}$$

To obtain only a single significant digit of accuracy, the number of trajectories needed is then

$$\mathcal{S}_{\text{min}} = \frac{100\sigma_v}{\overline{v}_\sigma} = 100\sqrt{e^{\sigma^2} - 1}. \tag{7.42}$$

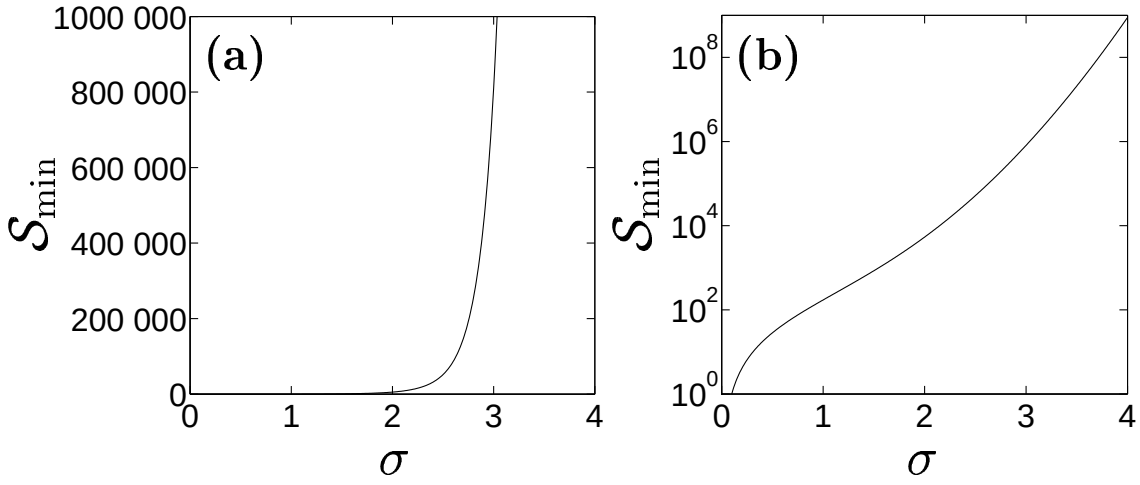

Figure 7.1: **Number of samples** $\mathcal{S}_{\min}$ required to obtain a single significant digit of precision in the mean of a random variable v_σ that is an exponential of a Gaussian random variable with standard deviation σ. Scales: **(a)** Linear, **(b)** logarithmic.

This minimum number of required samples (independent of v_0) is plotted in Figure 7.1. It can be seen there that for $\sigma \gtrsim 3$ the number of samples required becomes intractable, and this sets a practical limit on the variance of the logarithmic variable $v_L = \sigma\xi$:

$$\sigma^2 \lesssim \mathcal{O}(10)\,, \tag{7.43}$$

which will be referred to numerous times in this and following chapters.

At small standard deviations $\sigma \lesssim 1$, on the other hand, $\sigma_v \approx \sigma$, and the variance of the logarithmic and exponential variables ($\mathrm{var}[v_L]$ and σ_v^2, respectively) is approximately the same — a result that will also be useful.

Lastly, this sampling problem can also lead to systematic biases (but not boundary term errors) in averages of v with finite sample number $\mathcal{S}$ once $\sigma \gtrsim 3$, when (7.43) is violated. This is considered in detail in Appendix A.

Means of some combinations of Gaussian noises

Some expressions that will be used in Sections 7.5, and 7.8.2 are given below. Since they contain only odd powers of ξ,

$$\langle \sin(\sigma\xi) \rangle_{\mathrm{stoch}} = 0 \tag{7.44}$$

$$\langle \xi \cos(\sigma\xi) \rangle_{\mathrm{stoch}} = 0. \tag{7.45}$$

And, by the same series expansion approach as for (7.39)

$$\left\langle \xi e^{\sigma\xi} \right\rangle_{\text{stoch}} = \sigma \exp\left(\frac{\sigma^2}{2}\right) \tag{7.46}$$

$$\left\langle \cos(\sigma\xi) \right\rangle_{\text{stoch}} = \exp\left(-\frac{\sigma^2}{2}\right) \tag{7.47}$$

$$\left\langle \xi \sin(\sigma\xi) \right\rangle_{\text{stoch}} = \sigma \exp\left(-\frac{\sigma^2}{2}\right). \tag{7.48}$$

7.5 Optimization of diffusion gauges

7.5.1 Aims

Upon choice of the drift gauges (7.30) to remove the offending moving singularities, diffusion gauges can be chosen to vastly (as it turns out) improve the sampling behaviour of the simulation. The aim here will be to arrive at a diffusion gauge g'' for the one-mode system that satisfies the following:

1. Improves useful simulation times in the low-damped high boson occupation regime (this is the regime where simulations without diffusion gauges give very unsatisfactory results – see Figure 7.3 and Section 7.2.4).

2. Is easily generalized to many-mode situations. This means, in particular, that the gauge choice should allow for the possibility of mode occupations changing dynamically due to inter-mode coupling (although this is not actually seen in the one-mode toy system).

3. Is expressed as an exact expression, or does not require excessively involved calculations to evaluate. This is important, since in a simulation the gauge should be evaluated at each time step if it is to adapt to dynamically changing mode occupations.

4. Applies on timescales of the order of the coherence time (and shorter timescales as well). This is a relevant timescale only when mode occupations are larger than order unity, and is then smaller than the quantum revival time $t_{\text{revival}} = \pi/\chi$. At lower mean occupations (order unity or smaller), we require that the

simulation remains stable for a time $\mathcal{O}(1/\chi)$, which should be sufficient not to prematurely destabilize any coupled highly-occupied modes in multi-mode systems.

5. Depends only on variables in the current trajectory — i.e. on parameters of the current coherent-state projector $|\alpha\rangle\langle\beta^*|$ component of the full state $\widehat{\rho}$. This is necessary if we want to be able to parallelize the calculation, which enormously improves calculation times. Also, if the evolution of all possible coherent-state projectors can be stabilized to restrict distribution size and statistical error, then so will the evolution of all possible states since these are always expressed as a distribution, and estimated as an appropriate sample, of such projectors.

6. We are especially interested in the case of low or absent damping $\gamma \ll 2\chi$, since this is the regime where quantum effects are strongest, and also where the simulation is most unstable (see e.g. Sections 7.2.4 and 7.5.4). The highly-damped regime is a lesser priority, since there a mean-field, or other approximate simulation would be sufficient for most purposes.

This may seem like a lot of conditions for one quantity, but it helps to remember that g'' is in principle an *arbitrary* function.

7.5.2 Variables to be optimized

Before proceeding directly to searching for advantageous values of the diffusion gauge, there remain several more issues to address:

Which moment to optimize?

While, strictly speaking, this depends on which moment we might be interested in, in general we should concentrate on occupation number $\langle\widehat{n}\rangle$ or phase correlations $G^{(1)}$. If these basic low-order observables are badly calculated then higher-order observables will not do any better, because they are more sensitive to the distribution broadness.

Consider that estimators for these two observables are (by comparing their definitions (7.9) and (7.10) to observable estimators in the gauge P representation (5.10) and (5.13)) are

$$\langle \widehat{n} \rangle \propto \mathrm{Re}\left\{ \langle \Omega \breve{n} \rangle_{\mathrm{stoch}} \right\} \tag{7.49}$$

$$G^{(1)}(0,t) \propto \beta_0 \langle \Omega \alpha \rangle_{\mathrm{stoch}} \quad \text{or} \quad \propto \alpha_0^* \langle \Omega^* \beta^* \rangle_{\mathrm{stoch}} \tag{7.50}$$

(the normalization by denominators $\mathrm{Re}\left\{ \langle \Omega \rangle_{\mathrm{stoch}} \right\}$ has been omitted). One finds from (7.16) or (7.8) that both $d\breve{n}$ and $d\Omega$ are proportional to $e^{-g''}$, so varying the diffusion gauge g'' acts to scale noise in the number observable $\langle \widehat{n} \rangle \sim \langle \Omega \breve{n} \rangle_{\mathrm{stoch}}$ smoothly from very large at negative g'' to very small at positive g''. This does not suggest any "optimal" values of g''. On the other hand, the evolution of phase-dependent expectation values such as $G^{(1)}(0,t)$ displays high noise at both large negative and positive values of g'' but via different processes. (Large noise in $\Omega = e^{z_0}$ at negative g'', and large noise directly in α or β at positive values). This suggests that g'' parameterizes some tradeoff between phase-space and weight noise, and that there is some intermediate value of g'' at which the resulting uncertainty in phase observables is minimized. Thus optimization should be based on such phase variables.

Logarithmic variables

Ideally one would like to optimize for the variance of variables like $(\alpha\Omega)$, since these appear directly in the calculation of the observable $G^{(1)}$. Unfortunately, exact expressions for such variances are difficult to obtain in a closed form[2], and would probably be very complicated if obtained. A complicated form makes it difficult to arrive at an expression for the optimum g'' that would satisfy condition 3. in Section 7.5.1 (i.e. simple to evaluate during each simulation step).

It turns out, however, that exact expressions for the variances of the logarithms of phase-dependent observables such as $\mathrm{var}\left[\log(\alpha\Omega)\right] = \mathrm{var}\left[z_0 + n_L/2 + m_L/2\right]$ can

[2]The reason for this becomes clear after proceeding to calculate some logarithmic variances in (7.65). These require the evaluation of quantities such as $\langle n''(t')n''(t'')\rangle_{\mathrm{stoch}}$ given in (7.64). To evaluate $\mathrm{var}\left[\Omega\alpha\right] = \mathrm{var}\left[e^{G_L}\right]$, on the other hand, requires calculating averages of the form $\langle n''(t_1)n''(t_2)n''(t_3), \cdots \rangle_{\mathrm{stoch}}$ to all orders, which becomes increasingly involved as the number of factors grow.

be found with (relative) convenience and ease, and we will look for values of g'' to minimize this logarithmic variance instead of var $[\alpha\Omega]$.

As further justification of this choice, one can make an analogy between the behaviour of $\log\alpha$ and α, etc. versus the behaviour of the Gaussian random variable v_L of Section 7.4 and $v_\sigma = e^{v_L}$. In both cases the logarithmic variable is generated by Brownian motion, although in the $\log\alpha$ case, there is additional drift. One sees from (7.40) that for $\sigma \lesssim \mathcal{O}(1)$, the variances of both the logarithmic and "normal" variables are the same. This corresponds to short time evolution of the anharmonic oscillator in the above analogy. Furthermore, because of the rapid rise of variance with time, the range of σ for which $\sigma \not\approx \sigma_v$ but the simulation gives any useful accuracy is fairly narrow and occurs in the more noisy part of the simulation.

In summary, it can be expected that a optimization of g'' in logarithmic variances will still give good results. This is borne out by the massive improvement in simulation times seen in Figure 7.3. Certainly, however, some further improvement could be obtained by considering non-logarithmic variances (particularly since in the full simulation, $\log\alpha\Omega$ etc. are not exactly Gaussian distributed due to the effect of the drift terms), although it is not clear whether the difference would be significant or not.

Which phase-dependent variable to optimize

The first-order correlation function $G^{(1)}(0,t)$ can be estimated in two ways, as seen in (7.50). Hence, it is best to optimize for the average variance of the logarithm of the two random variables $\Omega\alpha\beta_0$ and $(\Omega\alpha_0\beta)^*$ corresponding to the $G^{(1)}$ estimate. Also, since general coherent state initial conditions to be optimized will have arbitrary phases, we should optimize a variance of variables related to $|G^{(1)}(0,t)|$ rather than the complex $G^{(1)}$.

7.5.3 Optimization of g''

$|G^{(1)}(0,t)|$ is estimated by either e^{G_L} or $e^{\widetilde{G}_L}$, where

$$G_L(t) = \mathrm{Re}\left\{\log\beta_0 + \log\alpha(t) + z_0(t)\right\} \tag{7.51a}$$

$$\widetilde{G}_L(t) = \mathrm{Re}\left\{\log\alpha_0 + \log\beta(t) + z_0(t)\right\}, \tag{7.51b}$$

while the uncertainty in the estimate will be proportional to $\mathrm{var}\left[e^{G_L}\right]$ or $\mathrm{var}\left[e^{\widetilde{G}_L}\right]$. Taking the considerations of the previous Section 7.5.2 into account, let us look for such $g'' = g''_{\mathrm{opt}}$ that the mean variance of G_L and $\widetilde{G}_L$ is minimized for the anharmonic oscillator system. This minimum occurs when

$$\frac{\partial\left(\mathrm{var}\left[G_L(t_{\mathrm{opt}})\right] + \mathrm{var}\left[\widetilde{G}_L(t_{\mathrm{opt}})\right]\right)}{\partial g''} = 0. \tag{7.52}$$

Note that the optimal value g''_{opt} will in general depend upon the target time $t_{\mathrm{opt}} = t$ at which the variances are considered.

The formal solution of the gauged anharmonic oscillator equations (7.33), assuming uniform initial weight $\Omega(0) = 1$, is straightforward to find:

$$n_L(t) = \log(n_0) - \gamma t + \sqrt{\chi}e^{-g''}\left[i\zeta^+(t) - \zeta^-(t)\right] \tag{7.53a}$$

$$m_L(t) = \log(\alpha_0/\beta_0) - 2i(\omega-\chi)t - 4i\chi\int_0^t n'(t')dt' + \sqrt{\chi}e^{g''}\left[i\zeta^-(t) - \zeta^+(t)\right] \tag{7.53b}$$

$$z_0(t) = -\sqrt{\chi}e^{-g''}\int_0^t n''(t')\left[\eta^+(t') + i\eta^-(t')\right]dt', \tag{7.53c}$$

where using the definition (7.27).

$$\eta^{\pm}(t) = \frac{dW_1(t)}{dt} \pm \frac{dW_2(t)}{dt} \tag{7.54}$$

are independent real Gaussian noises obeying

$$\left\langle\eta^{\pm}(t)\right\rangle_{\mathrm{stoch}} = 0 \tag{7.55a}$$

$$\left\langle\eta^{\pm}(t)\eta\pm(t')\right\rangle_{\mathrm{stoch}} = 2\delta(t-t') \tag{7.55b}$$

$$\left\langle\eta^{\pm}(t)\eta^{\mp}(t')\right\rangle_{\mathrm{stoch}} = 0, \tag{7.55c}$$

and so $d\eta = \sqrt{i}(\eta^- - \eta^+)\,dt/2$. Also,

$$\zeta^{\pm}(t) = \int_0^t \eta^{\pm}(t')dt'. \tag{7.56}$$

These $\zeta^{\pm}$ are time-correlated Gaussian random variables. Using (7.55), they obey the relationships

$$\left\langle \zeta^{\pm}(t) \right\rangle_{\rm stoch} = 0 \tag{7.57a}$$

$$\left\langle \zeta^{\pm}(t)\zeta\pm(t') \right\rangle_{\rm stoch} = 2\min\left[t,t'\right] \tag{7.57b}$$

$$\left\langle \zeta^{\pm}(t)\zeta^{\mp}(t') \right\rangle_{\rm stoch} = 0. \tag{7.57c}$$

The variables to optimize are

$$\left[\begin{array}{c} G_L \\ \widetilde{G}_L \end{array} \right] = \log|n_0| - \frac{\gamma}{2}\,t - \frac{\sqrt{\chi}}{2}\left(e^{-g''}\zeta^{-}(t) \left[\begin{array}{c} + \\ - \end{array} \right] e^{g''}\zeta^{+}(t) \right) - \sqrt{\chi}e^{-g''}\int_0^t n''(t')\eta^{+}(t')dt'. \tag{7.58}$$

In the Ito calculus the noises at t' are independent of any variables at t', so one finds

$$\left[\begin{array}{c} \langle G_L \rangle_{\rm stoch} \\ \langle \widetilde{G}_L \rangle_{\rm stoch} \end{array} \right] = \log|n_0| - \frac{\gamma}{2}\,t, \tag{7.59}$$

and using (7.57b)

$$\begin{aligned} \left[\begin{array}{c} \langle G_L^2 \rangle_{\rm stoch} \\ \langle \widetilde{G}_L^2 \rangle_{\rm stoch} \end{array} \right] = & \left[\begin{array}{c} \langle G_L \rangle_{\rm stoch}^2 \\ \langle \widetilde{G}_L \rangle_{\rm stoch}^2 \end{array} \right] + \chi t \cosh 2g'' \left[\begin{array}{c} + \\ - \end{array} \right] \chi \int_0^t \left\langle n''(t')\eta^{+}(t')\zeta^{+}(t) \right\rangle_{\rm stoch} dt' \\ & + \chi e^{-2g''} \int_0^t dt' \int_0^t dt'' \left\langle n''(t')n''(t'') \right\rangle_{\rm stoch} \left\langle \eta^{+}(t')\eta^{+}(t'') \right\rangle_{\rm stoch}, \end{aligned} \tag{7.60}$$

where use has also been made of the independence of $\eta^{\pm}(t')$ and $\zeta^{\mp}(t)$.

To further evaluate (7.60), one needs to calculate the averages containing n''. Define $c = \sqrt{\chi}e^{-g''}$, and $n_0 = n_0' + in_0''$. Firstly,

$$\begin{aligned} \left\langle n''(t) \right\rangle_{\rm stoch} &= e^{-\gamma t} \left\langle e^{-c\zeta^{-}} \right\rangle_{\rm stoch} \left[n_0' \left\langle \sin c\,\zeta^{+} \right\rangle_{\rm stoch} + n_0'' \left\langle \cos c\,\zeta^{+} \right\rangle_{\rm stoch} \right]. \\ &= n_0'' e^{-\gamma t} \end{aligned} \tag{7.61}$$

where we have first used the independence of the $\zeta^{\pm}$ to separate the stochastic averages, and then applied expressions (7.39), (7.44), and(7.47) to evaluate them.

Now, since noises at times $t > t'$ are uncorrelated with those at t' or earlier,

$$\begin{aligned}\left\langle n''(t')\eta^+(t')\zeta^+(t)\right\rangle_{\text{stoch}} &= \left\langle n''(t')\eta^+(t')\zeta^+(t')\right\rangle_{\text{stoch}} \\ &= \int_0^{t'} \left\langle n''(t')\eta^+(t')\eta^+(t'')\right\rangle_{\text{stoch}} dt'' \\ &= \int_0^{t'} \left\langle n''(t')\right\rangle_{\text{stoch}} \left\langle \eta^+(t')\eta^+(t'')\right\rangle_{\text{stoch}} dt'' \\ &= 2\left\langle n''(t')\right\rangle_{\text{stoch}}, \end{aligned} \tag{7.62}$$

using (7.55b).

Secondly, if $t'' > t'$, noting that

$$\zeta^{\pm}(t'') = \zeta^{\pm}(t') + \widetilde{\zeta}^{\pm}(t''-t'),$$

where the $\widetilde{\zeta}^{\pm}(t)$ are independent of the $\zeta^{\pm}(t)$, but have the same properties (7.57), one finds that

$$\begin{aligned}&\left\langle n''(t')n''(t'')\right\rangle_{\text{stoch}} \\ &= e^{-\gamma(t'+t'')}\left\langle e^{-2c\zeta^-(t')}\right\rangle_{\text{stoch}}\left\langle e^{-c\widetilde{\zeta}^-(t''-t')}\right\rangle_{\text{stoch}}\left\langle \cos c\,\widetilde{\zeta}^+(t''-t')\right\rangle_{\text{stoch}} \\ &\quad\times\left\{[n_0']^2\left\langle \sin^2 c\,\zeta^+(t')\right\rangle_{\text{stoch}}[n_0'']^2\left\langle \cos^2 c\,\zeta^+(t')\right\rangle_{\text{stoch}} + n_0'n_0''\left\langle \sin 2c\,\zeta^+(t')\right\rangle_{\text{stoch}}\right\}. \end{aligned} \tag{7.63}$$

Terms containing $\left\langle \sin c\,\widetilde{\zeta}\right\rangle_{\text{stoch}} = 0$ have already been discarded. Evaluating the averages using (7.39) and (7.47), one obtains

$$\left\langle n''(t')n''(t'')\right\rangle_{\text{stoch}} = \frac{e^{-\gamma(t'+t'')}}{2}\left\{|n_0|^2 e^{4t'c^2} - (n_0')^2 + (n_0'')^2\right\}. \tag{7.64}$$

Due to symmetry

$$\int_0^t dt' \int_0^t dt'' n''(t')n''(t'') = 2\int_0^t dt'' \int_0^{t''} dt'\; n''(t')n''(t''),$$

and substituting (7.64), (7.62), and (7.61) into (7.60) and (7.59), then integrating, one obtains

$$\begin{aligned}\begin{bmatrix} \text{var}\,[G_L(t)] \\ \text{var}[\widetilde{G}_L(t)] \end{bmatrix} &= \chi t\cosh(2g'')\begin{bmatrix} + \\ - \end{bmatrix} 2\chi n_0''\left(\frac{1-e^{-\gamma t}}{\gamma}\right) \\ &\quad +\chi e^{-2g''}|n_0|^2\left(\frac{e^{4\chi e^{-2g''}t}e^{-2\gamma t}-1}{4\chi e^{-2g''}-2\gamma}\right) - \chi e^{-2g''}[(n_0')^2-(n_0'')^2]\left(\frac{1-e^{-2\gamma t}}{2\gamma}\right). \end{aligned} \tag{7.65}$$

The optimum $g'' = g''_{\rm opt}$ can now in theory be calculated by imposing (7.52).

Since this would involve the solution of a transcendental equation, it would be cumbersome to use in a numerical simulation, going against requirement 3 of Section 7.5.1, because one would have to execute a time-consuming algorithm at each time step. By considering, below, some important special cases, an approximation to the optimum $g''_{\rm opt}$ applicable under the broad conditions aimed for in Section 7.5.1 will be found, which can then be easily used in actual simulations.

7.5.4 Important special cases

1. Perhaps the most important special case is when damping is absent ($\gamma = 0$). This is also the worst case in terms of simulation stability. At relatively short times one has

$$4\chi t_{\rm opt} e^{-2g''_{\rm opt}} \ll 1, \tag{7.66}$$

and the optimum is given (from (7.52) and (7.65)) by the roots of the cubic in $V_g = e^{-2g''_{\rm opt}}$:

$$8\chi t_{\rm opt}|n_0|^2 V_g^3 + [4(n_0'')^2 + 1]V_g^2 - 1 = 0. \tag{7.67}$$

In the usual case of simulations with sizeable occupation numbers in modes, and times up to coherence time (which then is much shorter than the quantum revival time π/χ) this short time condition is satisfied. A very useful expression

$$g''_{\rm opt} \approx \frac{1}{3}\log\left(|n_0|\sqrt{8\chi t_{\rm opt}}\right). \tag{7.68}$$

applies when the V_g^2 term is negligible. This occurs at long enough times when n_0 is large enough and mostly real: i.e. when $1 + 4(n_0'')^2 \ll (8\chi t_{\rm opt}|n_0|^2)^{2/3}$. So $\chi t_{\rm opt}$ must be at least $\gg 1/8|n_0|^2$ (a higher limit applies if $n_0'' \neq 0$).

The opposite case when n_0 is either too small, too imaginary, or the time is too short has the V_g^3 term negligible and leads to

$$g''_{\rm opt} \approx \frac{1}{4}\log\left[1 + 4(n_0'')^2\right]. \tag{7.69}$$

2. It can be seen that the long time behaviour of the variances depends on the "damping strength" parameter

$$q = 2\gamma - 4\chi e^{-2g''}. \tag{7.70}$$

When q is positive, the long time (i.e. $qt \gg 1$) behaviour of (7.65) is asymptotic to a linear increase

$$\begin{bmatrix} \text{var}\,[G_L] \\ \text{var}[\widetilde{G}_L] \end{bmatrix} \rightarrow \chi t \cosh 2g'' - b \tag{7.71}$$

where $b = \chi e^{-2g''}\{[(n_0')^2 - (n_0'')^2]/2\gamma - |n_0|^2/q\} \mp 2\chi n_0''/\gamma$ is a constant. This means that the sampling uncertainty grows relatively slowly, and long simulation times are possible. When q is negative, on the other hand, the long time behaviour is $\chi e^{-2g''}|n_0|^2 e^{|q|t}/|q|$, and we expect a rapid appearance of intractable sampling error after some time $|q|t \gg 1$.

The parameter q depends on the relative strengths of the nonlinearity and the damping, and determines the long time behavior of the statistical error. Note though that if damping is present, then for large enough diffusion gauge g'', q can always be made positive, and the linear (in t) variance regime can be reached with a choice $g'' \geq \log\sqrt{2\chi/\gamma}$.

3. An immediate extension to nonzero damping of expressions (7.67), (7.68) and (7.69) can be derived for times $|qt_{\text{opt}}| \ll 1$ to give the cubic

$$8\chi t_{\text{opt}}|n_0|^2 V_g^3 + a_2 V_g^2 - 1 = 0 \tag{7.72a}$$

where

$$\begin{aligned} a_2(n_0, \gamma t_{\text{opt}}) &= 1 + 4(n_0'')^2 \left(\frac{1 - e^{-2\gamma t_{\text{opt}}}}{2\gamma t_{\text{opt}}}\right) \\ &\quad -2|n_0|^2 \left(\frac{1 - 2\gamma t_{\text{opt}} + 2(\gamma t_{\text{opt}})^2 - e^{-2\gamma t_{\text{opt}}}}{\gamma t_{\text{opt}}}\right). \end{aligned} \tag{7.72b}$$

The expression (7.68) still applies at large enough and real enough n_0: i.e. when $a_2 \ll (8\chi t_{\text{opt}}|n_0|^2)^{2/3}$. In the opposite case of $a_2 \gg (8\chi t_{\text{opt}}|n_0|^2)^{2/3}$, one has

$$g''_{\text{opt}} \approx \frac{1}{4}\log(a_2). \tag{7.73}$$

7.5.5 Suggested approximate form of diffusion gauge

Guided by conditions 2, 4, 5, and 6, in Section 7.5.1, we can see that the choice of $g''_{\rm approx}$ for the anharmonic oscillator might depend on the four real parameters n'_0, n''_0, $\chi t_{\rm opt}$ and γ. Because of conditions 4 and 5, we are most interested in the regime of small γ, and either $\chi t_{\rm opt} \lesssim \mathcal{O}\left(1/2\sqrt{|n_0|}\right)$ when $|n_0| \gtrsim \mathcal{O}(1)$, or $\chi t_{\rm opt} \lesssim \mathcal{O}(1)$ when $n_0 \lesssim \mathcal{O}(1)$. These cases are covered by expression (7.72).

This can be most easily seen in the two limits $|n_0| \gg 1$ and $|n_0| \ll 1$ where for small γ, we have $qt_{\rm opt} \approx -2(\chi t_{\rm opt}/|n_0|)^{2/3}$ and $\approx -4\chi t_{\rm opt}/\sqrt{1+4(n''_0)^2}$ respectively. Hence the condition $|q|t_{\rm opt} \ll 1$ applies for target times $\chi t_{\rm opt} \ll |n_0|/2\sqrt{2}$ and $\ll \approx (1+2|n''_0|)/4$ respectively, which is roughly sufficient for low occupations, and more than sufficient for high occupations.

To obtain an explicit estimate for $g''_{\rm opt}$, one can either evaluate the roots of the polynomials (7.67) or (7.72) by standard expressions, which can be still quite complicated although reasonably rapid, or use the approximation

$$g''_{\rm approx} = \frac{1}{6}\log\left\{8|n_0|^2\chi t_{\rm opt} + a_2^{3/2}\right\}, \tag{7.74}$$

which reduces to (7.68) and (7.73) in their limits of applicability, and works very well in practice (see figures 7.3, 7.6, and 7.5).

The discrepancy Δ between (7.74) and the exact optimization obtained by solving (7.52) with (7.65) is shown for real n_0 for a wide range of parameters in Figure 7.2. Note that the ubiquitous $e^{-2g''}$ factor is, for small discrepancy, $e^{-2g''_{\rm opt}} \approx (1-2\Delta)e^{-2g''_{\rm approx}}$. It can be seen that for occupations $\gtrsim \mathcal{O}(10)$ and/or for times shorter than, or of the order of, singly-occupied coherence time the approximation is very good.

The diffusion gauge choice (7.74) will be used from here on.

7.5.6 Relationship between target time and mode occupation

The expression (7.74) was worked out under the conditions that the mean occupation of the mode is conserved. In coupled-mode simulations this is no longer the case, and

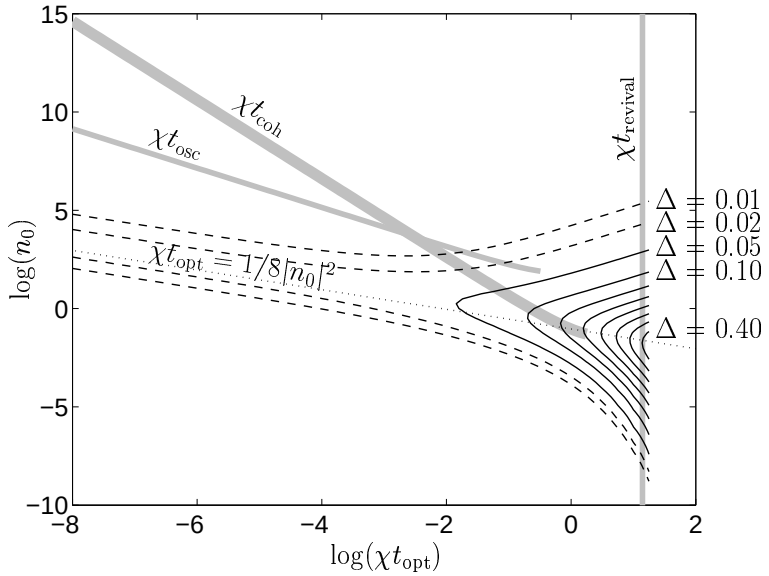

Figure 7.2: **Discrepancy** $\Delta = g''_{\rm opt} - g''_{\rm approx}$ between $g''_{\rm opt}$ (the exact optimization of g'' by solving (7.52) using (7.65)), and the approximate expression (7.74). Displayed is the case of no damping ($\gamma = 0$) and classical initial occupation ($n_0 = n'_0$), shown as a function of $t_{\rm opt}$ and n_0. Discrepancy values Δ are shown as SOLID CONTOURS with spacing 0.05. Additional DASHED CONTOURS shown at very low discrepancy. DOTTED LINE approximates region of greatest discrepancy $\chi t_{\rm opt} \approx 1/8{n'_0}^2$. For comparison, several physical timescales are also shown in GREY: time of first quantum revival $t_{\rm revival}$, phase coherence time $t_{\rm coh}$ and phase oscillation period $t_{\rm osc}$.

---

could be adapted for by replacing n_0 by $\breve{n}(t)$, which explicitly assumes independence of trajectories, and a Markovian process. Although the mean over all trajectories $\langle \Omega(t)\breve{n}(t)\rangle$ would be a better estimator of the mean boson occupation, this would be in conflict with aim 5 in Section 7.5.1, and might lead to biases due to complicated feedback mechanisms between trajectories.

Another assumption used to arrive at (7.74) was that g'' would be constant in time, which is now no longer the case. This raises the question of how to include the target time in $g''_{\rm opt}$. Two ways that quickly come to mind is either to calculate $g''_{\rm opt}(t)$

1. Always optimizing for a time $t_{\rm opt}$ forward from the present t (choosing then, explicitly, $g''_{\rm opt}(t_{\rm opt})$), or:

2. Optimizing for only the remaining time to the absolute target time $t_{\rm opt} \geq t$

(choosing, then, $g''_{\rm opt}(\max[t_{\rm opt}-t,0])$).

In combination, this gives rise to the four possible gauge forms (in the (7.74) approximation, using (7.72b))

$$g''_{\rm approx}(t) = \frac{1}{6}\log\left\{8|n_0|^2\chi t_{\rm opt} + a_2(n_0,\gamma t_{\rm opt})^{3/2}\right\}, \tag{7.75a}$$

$$g''_{\rm approx}(t) = \frac{1}{6}\log\left\{8|n_0|^2\chi t_{\rm rem} + a_2(n_0,\gamma t_{\rm rem})^{3/2}\right\}, \tag{7.75b}$$

$$g''_{\rm approx}(t) = \frac{1}{6}\log\left\{8|\breve{n}(t)|^2\chi t_{\rm opt} + a_2(\breve{n}(t),\gamma t_{\rm opt})^{3/2}\right\}, \tag{7.75c}$$

$$g''_{\rm approx} = \frac{1}{6}\log\left\{8|\breve{n}(t)|^2\chi t_{\rm rem} + a_2(\breve{n}(t),\gamma t_{\rm rem})^{3/2}\right\}(t), \tag{7.75d}$$

where the "remaining time to target" is

$$t_{\rm rem} = \max[t_{\rm opt}-t,0]. \tag{7.76}$$

These strategies have been numerically investigated for the undamped ($\gamma=0$) case with real n_0 starting conditions. It turns out that form (7.75d) has some advantage over the others, particularly at high occupations. Details are discussed in Section 7.7.1 and shown in Table 7.1.

7.5.7 Boundary term issues

When considering the use of an adaptive $g''(t,\breve{n}(t))$, one should be careful that the g'' dependent terms do not introduce new noise divergences that were not present when the standard $g''=0$ square root noise matrix B_0 was used[3]. The condition to avoid noise divergence symptoms (and so, presumably, boundary term errors) is as always (6.3): The stochastic equations should contain no radial component that grows faster than exponentially as large radial values of the phase-space variables are reached.

Since the suggested forms (7.75) depend directly only on the complex occupation variable $\breve{n}=e^{n_L}$, and not on either of the other independent variables (m_L, and z_0), then it suffices to only check that the $\breve{n}$ evolution equation contains no radial super-exponential growth. This is because the g'' dependent terms in the m_L and z_0

[3]Incidentally, any boundary term errors introduced by such noise divergences would have to be of the second kind, since the choice of diffusion gauge is made at the level of the FPE-stochastic equation correspondence, long after any boundary terms $\widehat{\mathcal{B}}$ has been discarded.

evolutions simply accumulate integrals of functions of n_L, and if $\breve{n}$ remains finite, then so will the other variables.

The $\breve{n}$ evolution is now

$$\begin{aligned} d\breve{n} &= 2i\breve{n}\sqrt{i\chi}e^{-g''}d\eta + \gamma(\overline{n}_{\rm bath} - \breve{n})\,dt \\ &\quad +(\varepsilon\,dt + \sqrt{\gamma\overline{n}_{\rm bath}}\,d\eta_{\rm bath})\beta + (\varepsilon\,dt + \sqrt{\gamma\overline{n}_{\rm bath}}\,d\eta_{\rm bath})^*\alpha. \end{aligned} \tag{7.77}$$

Provided the time dependence of parameters $\gamma, \overline{n}_{\rm bath}, \varepsilon$, or χ is not pathological, the condition (6.3) means g'' must obey

$$\lim_{|\breve{n}(t)|\to\infty} e^{-g''} \propto |n(t)|^a \text{ where } a \leq 0. \tag{7.78}$$

for no super-exponential growth to occur. That is, $e^{g''}$ must grow as a non-negative power law (or faster) as $|\breve{n}|$ becomes large. This is seen to be satisfied by the suggested forms (7.75). Finally, non g''-dependent terms were considered in Section 7.3, and found not to lead to any moving singularities.

It is concluded, then, that the diffusion gauge form (7.74) does not lead to any new noise divergences or moving singularities, and hence none of the usual boundary term error symptoms have been reintroduced.

7.5.8 Particle gain

External particle gain (rather than loss due to a zero-temperature heat bath) complicates the behaviour. Looking at (7.77), the bath interactions tend to equilibrate the mode occupation to the bath value $\overline{n}_{\rm bath}$. If $\overline{n}_{\rm bath} \ll \langle\widehat{n}\rangle$, then one can expect that the optimum gauge calculated with nonzero γ will be largely unchanged. For highly occupied bath modes, or strong coherent particle gain ε, a new analysis of g'' optimization may give better results that (7.75), however this appears to be a very involved procedure. An obvious first try is to just see what happens with the gauge form (7.75).

7.6 Estimates of simulation times

The limit (7.43) on the variance of exponentials of Gaussian random variables can be used to estimate times of useful simulation $t_{\rm sim}$ from expressions for $\mathrm{var}\,[G_L]$ — since G_L behaves much like a Gaussian random variable in analogy to $\sigma\xi$, and observables are estimated by e^{G_L} in analogy to $v_\sigma \propto e^{\sigma\xi}$. Imposing

$$(\mathrm{var}\,[G_L(t_{\rm sim})] + \mathrm{var}[\widetilde{G}_L(t_{\rm sim})])/2 \approx 10, \tag{7.79}$$

one can solve for $t_{\rm sim}$ to obtain at estimate at least of the scaling of $t_{\rm sim}$ with system parameters.

Consider first the **gauged** simulation. For coherent state initial conditions $\beta_0 = \alpha_0^*$ at small damping $\gamma t \ll 1$, and short enough times $|q|t \ll 1$,

$$\mathrm{var}\,[G_L] = \frac{\chi t}{2}\left(V_g + \frac{1}{V_g}\right) + 2(\chi V_g t n_0')^2. \tag{7.80}$$

For large particle number $n_0' \gg 1$, $g''_{\rm opt}$ takes the form (7.68), so $V_g \approx 1/2(n_0'^2\chi t)^{1/3}$, the $\chi t V_g/2$ term is negligible, and $\mathrm{var}\,[G_L] \approx 3(n_0'\chi^2 t^2)^{2/3}/2$, and (7.79) leads to a useful simulation time

$$t_{\rm sim} \approx \frac{(20/3)^{3/4}}{\chi\sqrt{n_0'}} \approx \mathcal{O}\left(10\, t_{\rm coh}\right). \tag{7.81}$$

Since in this regime $|q|t \approx 4\chi t V_g \approx 2(\chi t/n_0')^{2/3}$, then $|q|t_{\rm sim} \approx \mathcal{O}\left(5\right)/n_0' \ll 1$, and so the expression (7.81) is consistent with the original short time assumption $|q|t \ll 1$ when $n_0' \gg \mathcal{O}\left(5\right)$.

At small occupations $n_0' \ll 1$ on the other hand, $g''_{\rm opt} \to 0$, and at long times, $\mathrm{var}\,[G_L] \approx \frac{1}{4}n_0'^2 e^{4\chi t}$. Thus useful simulation time scales very slowly with n_0', and is

$$t_{\rm sim} \approx \frac{\mathcal{O}\left(1\right) - \frac{1}{2}\log n_0'}{\chi}. \tag{7.82}$$

The "long time" condition holds while $\frac{1}{4}n_0'^2 e^{4\chi t}$ is much greater than the lower order term χt. That is, $n_0' \gg \mathcal{O}\left(10^{-8}\right)$. At even smaller n_0', the χt term dominates (7.80), and

$$t_{\rm sim} \approx \mathcal{O}\left(10\right)/\chi. \tag{7.83}$$

For comparison, consider the **positive P** behaviour, which can be estimated from the logarithmic variances (7.92) for the case with no drift gauge, which are worked out in Section 7.8.2. For coherent state initial conditions $n_0 = n_0'$ and small damping $\gamma t \ll 1$,

$$\mathrm{var}\,[G_L] \approx \chi t + 2n_0'(\chi t)^2 + 2\chi^2 {n_0'}^2 \left\{ \frac{e^{4\chi t} - 1}{8\chi^2} - \frac{t}{2\chi} - t^2 \right\}. \tag{7.84}$$

At short times $4\chi t \ll 1$ the leading term in the $\{\bullet\}$ expression is $\frac{8}{3}(\chi t)^3 {n_0'}^2$. In such a case, for large mode occupation $n_0' \gg \mathcal{O}(1)/\chi t$ this term dominates, and using (7.79), one obtains

$$t_{\mathrm{sim}} \approx \frac{\mathcal{O}(1)}{\chi {n_0'}^{2/3}}. \tag{7.85}$$

Checking back, $1/\chi t \approx \mathcal{O}(1)\, {n_0'}^{2/3}$, so (7.85) is consistent with the short time assumption for $n_0' \gg 1$. At long times, one again has (7.82) and (7.83). The expression (7.85) is also useful in estimating simulation times for many-mode models, as will be seen in Section 10.2.1.

Curiously, the "stable" drift-gauged simulation with **no diffusion gauge** does even worse than the positive P. In this case, $V_g = 1$, and using (7.80), at large n_0'

$$t_{\mathrm{sim}} \approx \frac{\mathcal{O}(2)}{\chi n_0'} \approx t_{\mathrm{osc}}, \tag{7.86}$$

which is consistent when $n_0' \gg \mathcal{O}\left(\frac{1}{4}\right)$.

The numerical results in Table 7.1 and Figure 7.3, are seen to agree with these estimates to within constant factors of $\mathcal{O}(1)$.

7.7 Numerical investigation of improvement

To unambiguously determine the improvements in simulation time that are achieved by the use of the proposed gauges, simulations of an undamped anharmonic oscillator were carried out for a wide range of mode occupations and a variety of gauges, testing various target times t_{opt} where appropriate. (The undamped system was chosen because this is the worst case.)

Figure 7.3 compares t_{sim}, the maximum time achieved with various methods at which useful precision in the phase correlations $G^{(1)}(0,t)$ can be obtained. Note

the logarithmic scale. Results at high boson occupation are tabulated in Table 7.1, which includes data for a larger set of gauge choices. Figure 7.6 gives examples of calculated values $|G^{(1)}(0,t)|$ along with error estimates. Table 7.2 gives some empirical fitting parameters to expression (7.89) for the useful simulation time $t_{\rm sim}$. These may be useful to assess simulation times when the particle occupation is of $\mathcal{O}(10)$ or smaller, and the expressions (7.81) or (7.85) are not accurate.

Details of the sampling error behaviour are shown in Figure 7.5 for a range of gauge choices, while Figure 7.4 shows the dependence of useful simulation times on the target time parameter $t_{\rm opt}$ for a variety of gauge forms for two example mode occupations: $n_0 = 1$ and $n_0 = 10^4$.

7.7.1 Procedure

Simulations were carried out with coherent state initial conditions for a wide range of mean occupation number

$$n_0 = \{10^{-5}, 10^{-4}, 10^{-3}, 0.01, 0.1, 1, 10, 100, 1000, 10^4, 10^5, 10^6, 10^8, 10^{10}\}. \quad (7.87)$$

The following gauges, and their varieties as seen in Table 7.1, were tried for each n_0 value:

i) No gauge: $\mathcal{G}_k = g'' = 0$. This is the standard positive P distribution technique.

ii) Drift gauge only: $\mathcal{G}_k$ given by (7.30), and $g'' = 0$.

iii) Both drift gauge (7.30) and diffusion gauges of the four related forms (7.75).

iv) Diffusion gauge (7.100) only, as described by Plimak *et al*[2] (See Section 7.9.2).

v) Drift gauge (7.99) only, as described by Carusotto *et al*[1] (See Section 7.9.1)

vi) Adaptive diffusion gauges (7.94) only (of the four forms (7.97)), and $\mathcal{G}_k = 0$.

For the diffusion gauges of iii), iv), and vi), which depend on an *a priori* target time parameter $t_{\rm opt}$, a wide variety of target times were tried to investigate the dependence between $t_{\rm sim}$ and $t_{\rm opt}$, and ascertain what are the longest simulation times achievable. The dependence of $t_{\rm sim}$ on $t_{\rm opt}$ is plotted in Figure 7.4, while the best times are tabulated in Tables 7.1, 7.2, and Figure 7.3.

The term *useful* precision has been taken to indicate a situation where the estimate $\overline{O}$ of the expectation value of some observable $\widehat{O}$ is known to be precise to at least one significant digit when $\mathcal{S} = 10^6$ trajectories are used. That is, $\Delta\overline{O}(\mathcal{S} = 10^6) \leq |\overline{O}|/10$. Since for many-mode systems, the calculation of even one trajectory is reasonably time consuming, it is clear that $\mathcal{S} = 10^6$ trajectories is very unlikely to be exceeded for most non-trivial problems. Hence, meaningful results for non-trivial problems are at best likely to be obtained only in the parameter region where the above-defined "useful" precision condition is satisfied. If one calculates some lesser (than 10^6) number of trajectories, yet $\mathcal{S} \gg 1$, then the Central Limit theorem can be used to extrapolate $\Delta\overline{O}$ to the situation when $\mathcal{S} = 10^6$, since $\Delta\overline{O} \propto 1/\sqrt{\mathcal{S}}$. This gives finally, that the precision is taken to be "useful" when

$$\Delta\overline{O}(\mathcal{S})\sqrt{\frac{\mathcal{S}}{10^6}} \leq \frac{1}{10}|\overline{O}|. \tag{7.88}$$

In the current simulations, the observable in question is $|G^{(1)}(0,t)|$, and the "simulation time" $t_{\rm sim}$ that will be referred to here is the maximum time at which useful precision in $|G^{(1)}(0,t)/G^{(1)}(0,0)|$ is retained. Each actual simulation was done with $\mathcal{S} = 10^4$ trajectories.

Uncertainties in the calculated useful simulated times arise because the $\Delta|G^{(1)}|$ are themselves estimated from the finite ensemble of $\mathcal{S}$ trajectories. The uncertainty in $\Delta|G^{(1)}|$ was estimated by inspection of several (usually 10) independent runs with identical parameters. The range of values of $t_{\rm sim}$ seen was taken to be twice the uncertainty in $t_{\rm sim}$.

The scalings of simulation time with particle number for $n_0' \gg 1$ and $n_0' \ll 1$ have been worked out in Section 7.6. Taking these results into account, Table 7.2 empirically fits the simulation time $t_{\rm sim}$ to

$$t_{\rm est} = \frac{1}{\chi}\left\{\left[c_1 {n_0'}^{-c_0}\right]^{-c_2} + \left[\log\left(\frac{e^{c_3}}{{n_0'}^{c_4}} + 1\right)\right]^{-c_2}\right\}^{-1/c_2} \tag{7.89}$$

for intermediate times, as this may be useful for evaluation of simulation strategies in a many-mode case. c_0 characterizes the power-law scaling of $t_{\rm sim}$ at high occupation, c_1 the pre-factor for high n_0', c_3 a constant residual $t_{\rm sim}$ at near vacuum, c_4 characterizes the curvature at small n_0', while c_2 is related to the stiffness of the transition.

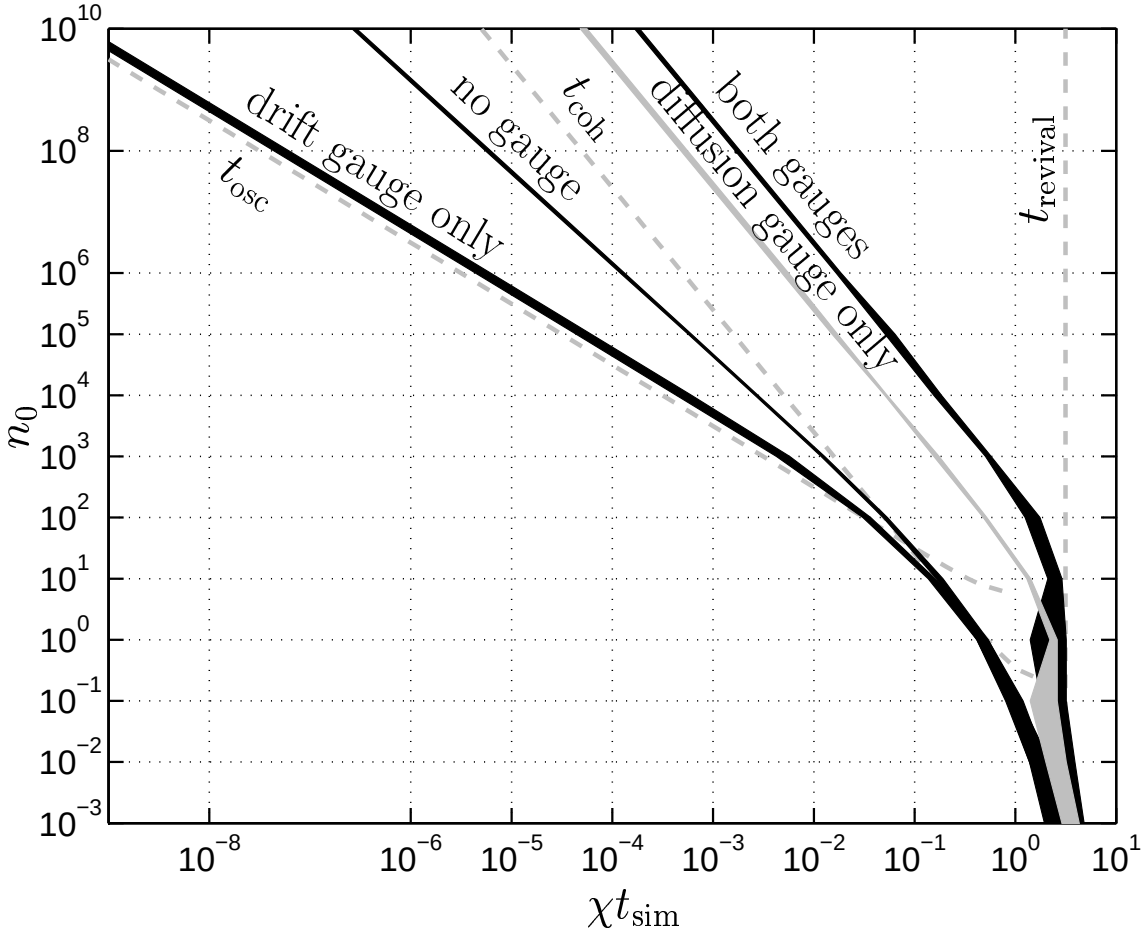

Figure 7.3: **Maximum useful simulation time** $t_{\rm sim}$, of the one-mode undamped anharmonic oscillator with various gauge choices. Initial coherent state mean mode occupations $n_0 = n_0'$. Width of plotted lines shows estimated uncertainty in the values shown. The DRIFT GAUGE is (7.30), while the DIFFUSION GAUGE is (7.100) of Plimak *et al*[2] when on its own, or (7.75d) when with the drift gauge (7.30). For comparison, several timescales from Section 7.2.3 are also shown as broken lines: time of first quantum revival $t_{\rm revival}$, phase coherence time $t_{\rm coh}$ and phase oscillation period $t_{\rm osc}$.

The expression (7.89) reduces to $c_1 {n_0'}^{-c_0}/\chi$ and $(c_3 - c_4 \log n_0')/\chi$, when $n_0' \gg 1$ and $n_0' \ll 1$, respectively, in agreement with the limiting expressions (7.81) and (7.82). Uncertainty Δc_j in parameters c_j was worked out by requiring $\sum_{n_0}\{[t_{\rm est}(c_j \pm \Delta c_j, n_0) - t_{\rm sim}(n_0)]/\Delta t_{\rm sim}\}^2 = \sum_{n_0}\{1 + ([t_{\rm est}(c_j, n_0) - t_{\rm sim}(n_0)]/\Delta t_{\rm sim})^2\}$. In the range checked ($n_0 \in [10^{-5}, 10^{10}]$), the fit is good — i.e. there are no outlier data that would lie significantly beyond the range of $t_{\rm est}$ specified by parameters $c_j \pm \Delta c_j$.

Table 7.1: **Maximum simulation time**, at useful precision, of the one-mode system in the limit $(n_0 = n_0') \gg 1$, achievable with various gauge choices. Calculations are for the undamped ($\gamma = 0$) system, which is the worst case in terms of sampling error. More details are given in Section 7.7.1. For comparison, several timescales from Section 7.2.3 are also given: time of first quantum revival t_{revival}, phase coherence time t_{coh} and phase oscillation period t_{osc}.

Drift gauge $\mathcal{G}_k$	Diffusion gauge g''	Useful simulation time t_{sim} when $n_0 = n_0' \gg 1$	Maximum n_0 for which $\chi t_{\text{sim}} \geq 1$
$t_{\text{osc}} = \pi/\chi n_0'$			
(7.99)	0	$(1.06 \pm 0.16)\, t_{\text{osc}}$	$0.014\ ^{+\ 0.016}_{-\ 0.008}$
(7.30)	0	$(1.7 \pm 0.4)\, t_{\text{osc}}$	$0.08\ ^{+\ 0.07}_{-\ 0.05}$
0	**0**	$(\mathbf{1.27 \pm 0.08})\, /\chi {n_0'}^{2/3}$	0.11 ± 0.06
$t_{\text{coh}} = 1/2\chi\sqrt{n_0'}$			
0	(7.100) or (7.97a) or (7.97c)	$(8.2 \pm 0.4)\, t_{\text{coh}}$	12 ± 3
0	(7.97b) or (7.97d)	$(10.4 \pm 0.7)\, t_{\text{coh}}$	19 ± 4
(7.30)	(7.75b)	$(25.6 \pm 1.0)\, t_{\text{coh}}$	120 ± 30
(7.30)	(7.75a)	$(30 \pm 3)\, t_{\text{coh}}$	150 ± 40
(7.30)	(7.75c)	$(32 \pm 3)\, t_{\text{coh}}$	190 ± 15
(7.30)	(7.75d)	$(\mathbf{35 \pm 4})\, t_{\text{coh}}$	240 ± 70
$t_{\text{revival}} = \pi/\chi$			

Table 7.2: **Empirical fitting parameters** for maximum useful simulation time t_{sim} with several gauge choices. The fit is to expression (7.89).

	Positive P	Both gauges	Drift gauge	Diffusion gauge
Drift Gauge	0	(7.30)	(7.30)	0
Diffusion Gauge	0	(7.75d)	0	(7.97d)
c_0	2/3	1/2	1	1/2
c_1	1.27 ± 0.08	17.6 ± 1.7	5.5 ± 1.2	5.2 ± 0.4
c_2	$3.2 \pm {}^{\infty}_{1.2}$	$3.6 \pm {}^{\infty}_{2.3}$	$1.4 \pm {}^{\infty}_{0.4}$	$2.7 \pm {}^{\infty}_{1.0}$
c_3	-0.5 ± 0.3	2.8 ± 0.9	-0.5 ± 0.3	-2.4 ± 0.6
c_4	0.45 ± 0.07	0.23 ± 0.13	0.49 ± 0.08	0.23 ± 0.13

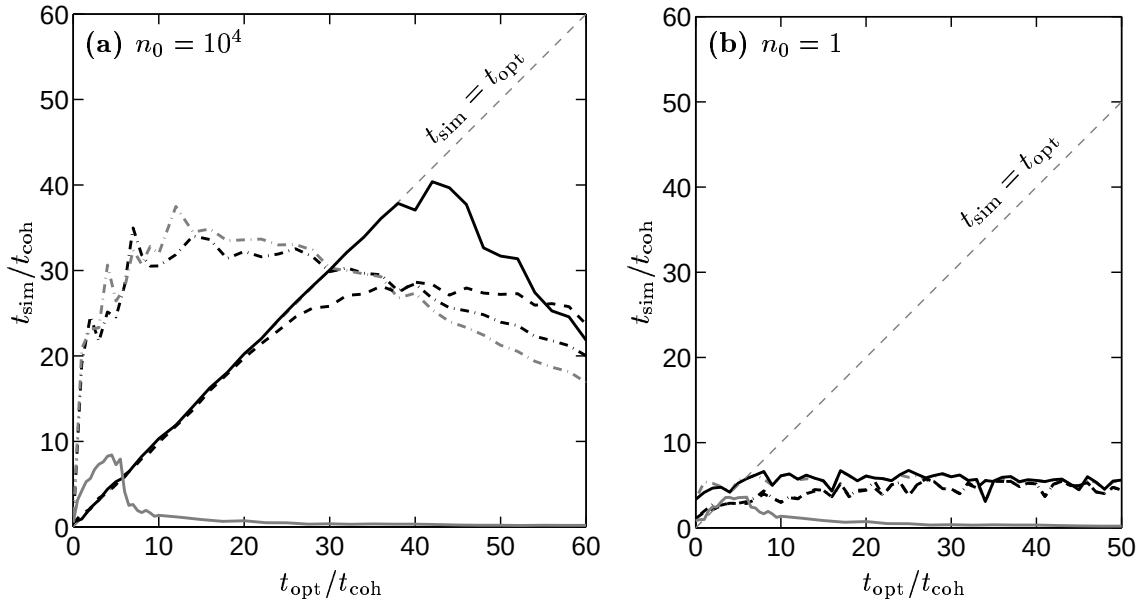

Figure 7.4: **Comparison of** *a priori* **target time $t_{\rm opt}$ with actual useful simulation time** $t_{\rm sim}$ for a variety of diffusion gauges: Results for drift gauges (7.30) with the four g'' forms (7.75) are shown as: (7.75d) – SOLID DARK; (7.75c) – DASH-DOTTED LIGHT; (7.75b) – DASHED; (7.75a) – DASH-DOTTED DARK. Relationship obtained using the diffusion gauge (7.100) of Plimak *et al*[2] (but no drift gauge) is also shown (SOLID LIGHT). The dashed line in the background shows, for reference $t_{\rm opt} = t_{\rm sim}$. Subplot **(a)**: mean particle number $n_0 = 10^4$, **(b)**: $n_0 = 1$.

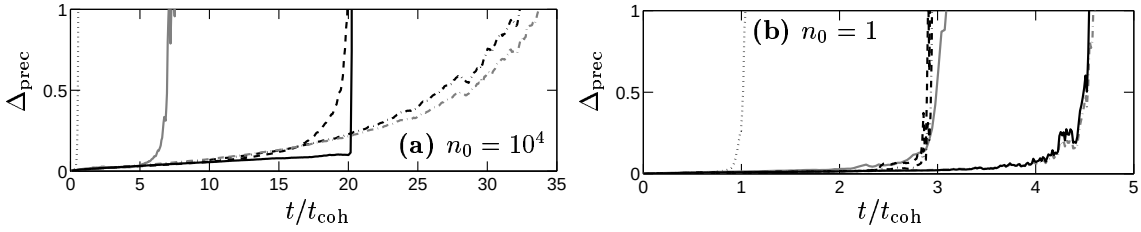

Figure 7.5: **Uncertainty in** $|G^{(1)}(0,t)|$, as a function of time. The quantity plotted is $\Delta_{\rm prec} = \sqrt{\mathcal{S}/10^6}(10\ \Delta|G^{(1)}(0,t)|\ /\ |G^{(1)}(0,0)|)$, so that $\Delta_{\rm prec} \leq 1$ corresponds to useful precision as defined in Section 7.7.1. Results are plotted for combined drift (7.30) and diffusion (7.75) gauges, where the four forms are shown as : (7.75d) – SOLID DARK; (7.75c) – DASH-DOTTED LIGHT; (7.75b) – DASHED; (7.75a) – DASH-DOTTED DARK. Data for the diffusion gauge (7.100) of Plimak *et al*[2] with $t_{\rm opt} = 3t_{\rm coh}$ as used therein is shown as a LIGHT SOLID line, while the ungauged positive P calculation is shown as a DOTTED line. Simulations were carried out with $\mathcal{S} = 10^4$ trajectories, starting with initial coherent state conditions: **(a)** $n_0 = 10^4$ **(b)** $n_0 = 1$. The combined drift-and-diffusion-gauge plots were calculated with target times of: **(a)** $t_{\rm opt} = 20t_{\rm coh}$ **(b)** $t_{\rm opt} = 4t_{\rm coh}$.

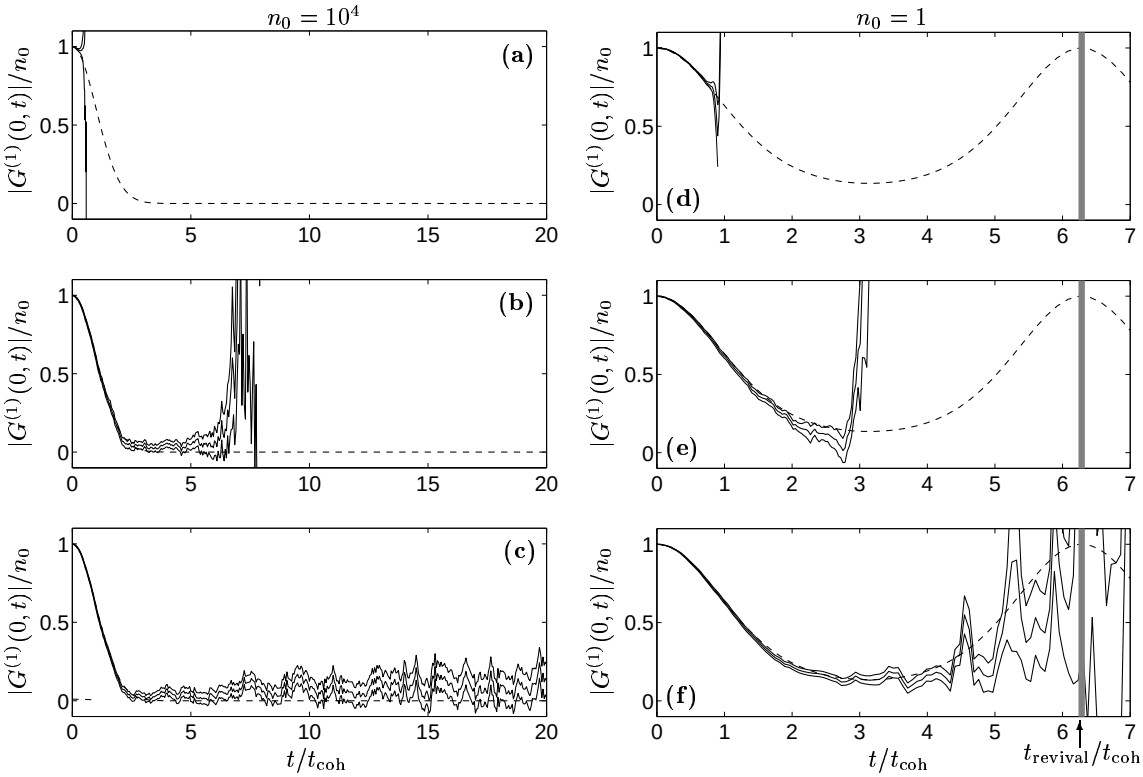

Figure 7.6: **Modulus of the phase correlation function** $G^{(1)}(0,t)$. Comparison of calculations with different gauges: Subplots **(a)** and **(d)**: Ungauged positive P. Subplots **(b)** and **(e)**: Diffusion gauge (7.100) of Plimak *et al*[2] with $t_{\rm opt} = 3t_{\rm coh}$. Subplots **(c)** and **(f)**: Combined drift and diffusion gauges (7.30) and (7.75d) with the choice $t_{\rm opt} = 20\,t_{\rm coh}$ The initial conditions were a coherent state with $\langle \widehat{n} \rangle = n_0$, where in subplots **(a)-(c)**: $n_0 = 10^4$ particles, and **(d)-(f)**: $n_0 = 1$. Triple SOLID lines indicate $G^{(1)}$ estimate with error bars. Exact values are also shown (single DASHED LINE). The quantum revival time is shown SHADED for the $n_0 = 1$ plots. $\mathcal{S} = 10^4$ trajectories in all cases

7.7.2 Features seen

- Combining drift and diffusion gauges gives the longest useful simulation times. Such simulations give good precision well beyond the point at which all coherence has decayed away for highly-occupied modes - potentially up to about 35 coherence times.

- Diffusion-gauge-only simulations also give quite good statistical behaviour (although useful simulation times are about 4 times shorter at high occupation than with both gauges).

- Despite the efficient behaviour of combined gauge simulations, using only a drift-gauge gives even worse statistical error than no gauge at all (although, this does eliminate potential boundary term systematics in a multi-mode system, which are a problem with no gauge). Such simulations are restricted in time to about one phase oscillation.

- Plain positive P simulations at high occupation last for about ${n'_0}^{1/3}$ phase oscillation periods, which is much less that the time required for significant coherence to be lost if n_0 is large.

- The diffusion gauge forms (7.75b) and (7.75d) that optimize for the "remaining time to target" $(t_{\rm opt} - t)$ show statistical errors that are well controlled by the choice of the target time $t_{\rm opt}$. Basically statistical error can be reliably expected to remain small up to the explicit target time $t_{\rm opt}$, provided that this is within the useful simulation range given in Table 7.1 — see Figure 7.5. Thus, a heuristic approach to get the maximum time out of a simulation would be to

  1. Pick $t_{\rm opt}$ to be some time that one wants to be able to simulate to.
  2. Run a simulation, and see how long useful observable estimates occur: $t_{\rm sim}(t_{\rm opt})$.
  3. Choose:
     (a) If $t_{\rm sim}(t_{\rm opt}) < t_{\rm opt}$ then reduce $t_{\rm opt}$ to some value between $t_{\rm sim}(t_{\rm opt})$ and the present $t_{\rm opt}$. Using this new value should give a new better simulation time also in that range. Iterate back to step 2. Or,
     (b) if $t_{\rm sim}(t_{\rm opt}) \approx t_{\rm opt}$ then either keep the simulation if one is happy with it, or one can try to increase $t_{\rm opt}$ to perhaps obtain more simulation time, going back to step 2.

  The rest of the diffusion gauge forms (7.75) do not follow such a simple dependence and appear to require tedious parameter searching to find the best gauge parameter choice for given initial conditions.

- Simulations showing quantum revivals have not been achieved. Generally it appears that useful simulation times are proportional to coherence times at high occupations. In this context, however, it is worth mentioning that quantum revivals *have* been seen in this system by Dowling[69] using the gauge P representation, by imposing externally-induced time reversal in the mode at a time t_{reversal}, where $t_{\text{coh}} < t_{\text{reversal}} \ll t_{\text{revival}}$. The phase coherence was seen by Dowling[69] to decay and then revive at $t = 2t_{\text{reversal}}$. This indicates that the potential for quantum revivals in these stochastic simulations is there, just not realized in the free evolution analyzed in this chapter.

- At low occupation, i.e. of the order of one boson or less, combined-gauge methods still give the best results, but the magnitude of their advantage becomes smaller.

- Of the four gauge forms (7.75), the form (7.75d) gives the longest useful simulations.

- The diffusion gauge forms (7.75d) and (7.75c) optimizing depending on the occupation of the current trajectory do better than those optimizing on the basis of only the initial condition. This is not surprising, since this approach is simply better tailored to the predicted subsequent evolution of each trajectory.

- At low occupations, a broad range of t_{opt} choices give much the same statistical behaviour. This is most likely because the forms (7.75) are not always the best optimizations of (7.65) in this regime for two reasons: 1) Because the "small time" condition $|q|t \ll 1$ is not always satisfied at the long time end of the simulation, and 2) because as seen in Figure 7.2, the form (7.74) is not an accurate root of the cubic (7.72).

- The simulation times with diffusion gauges (whether accompanied by drift gauge (7.30) or not) not only have better scaling with n_0 when n_0 is large, but this power-law decay of simulation time starts much later, as seen in Figure 7.3 and the right hand column of Table 7.1.

7.8 Diffusion gauges on their own

7.8.1 Motivation

The previous Sections 7.5 to 7.7 considered optimization of the diffusion gauge given that instabilities in the equations have been removed using the drift gauge (7.30). An approach that could be an alternative is to only use a diffusion gauge g'' to make a tradeoff between noise in the number and phase variables as before, but without introducing any drift gauge.

Such an approach could have the advantage that no weight spread is introduced since $dz_0 = 0$. The weight spread is not a major issue in a single-mode system, and clearly from Table 7.1 the drift-gauged simulations last longer, but with many modes there may be a problem: *All* the gauges introduce modifications to the *same* single weight variable. A vivid example occurs if we have M identical but independent modes. Then, $dz_0 = \sum_{k=1}^{2M} \mathcal{G}_k dW_k$, and the standard deviation of dz_0 is $\sqrt{M}$ times greater than for a single mode but with no new physics. Since the log-weight z_0 enters into the observable estimates in exponential fashion, the situation is again analogous to the average of an exponential of a Gaussian random variable, and there is the non-scalable useful simulation limit $\mathrm{var}\,[z_0] \lesssim \mathcal{O}\,(10)$ by condition(7.43). Since $\mathrm{var}\,[z_0(t)] \approx\propto Mt$ at short times, this translates to

$$t_{\mathrm{sim}} \propto \frac{1}{M} \tag{7.90}$$

in a worst case.

The major disadvantage of the $\mathcal{G} = 0$ approach, is that boundary term errors cannot be ruled out, as in the plain positive P method. One can, however, try to monitor for their appearance using the indicators developed by Gilchrist *et al*[64]: Spiking in moment calculations, rapid onset of statistical error after some time, or power-law distribution tails. A caveat is that these indicators tend to emerge only for fairly large ensemble sizes $\mathcal{S}$ (Typically what happens is that the indicators appear with a certain delay time if $\mathcal{S}$ small).

This $\mathcal{G} = 0$ method variant, although less desirable due to the need for careful monitoring of the simulation, was found to be much more successful than the

drift-gauged method (in its present form) at increasing simulation times for the preliminary example many-mode models simulated in Chapter 10.

7.8.2 Optimization of g'' and comments

Proceeding as before in Section 7.5.3, the formal solution of the anharmonic oscillator equations with $\Omega(0) = 1$ are as (7.53), but with the changes

$$m_L = (7.53\text{b}) + 4\chi \int_0^t n''(t')\, dt \tag{7.91a}$$

$$z_0(t) = 0. \tag{7.91b}$$

Following the same procedure as before, one obtains

$$\begin{bmatrix} \text{var}\,[G_L] \\ \text{var}[\widetilde{G}_L] \end{bmatrix} = \chi t \cosh(2g'') - 4\chi^2 \left(n_0' \begin{bmatrix} - \\ + \end{bmatrix} n_0'' e^{-2g''} \right) \left\{ \frac{1 - e^{-\gamma t}(1+\gamma t)}{\gamma^2} \right\}$$
$$+4\chi^2 |n_0|^2 \left\{ \frac{e^{-qt} - 1}{q(q-\gamma)} - \frac{1 - e^{-\gamma t}}{\gamma(\gamma - q)} - \frac{1}{2}\left(\frac{1 - e^{-\gamma t}}{\gamma} \right)^2 \right\}, \tag{7.92}$$

where the "damping strength" q is given by (7.70). The variational condition (7.52) can now be used to optimize g''.

Considering the same special cases as in Section 7.5.4,

1. With damping absent, and at relatively short times $|q|t \ll 1$, the optimized gauge is

$$g''_{\text{opt}} \approx g_{\text{approx}} = \frac{1}{4} \log \left[\frac{1}{3} (4\chi t_{\text{opt}} |n_0|)^2 + 1 \right]. \tag{7.93}$$

   (no cubic polynomial this time.)

2. The long time behaviour when $|q|t \gg 1$: When $q > 0$, the increase in the variances of G_L and $\widetilde{G}_L$ is still linear just like in (7.71), but with the constant $b = 4\chi^2|n_0|^2(q/2\gamma - 1)/q\gamma - 4\chi^2[n_0' \mp n_0'' e^{-2g''}]/\gamma^2$. When $q < 0$ the long time behaviour is again exponential: $G_L \approx 4\chi^2 |n_0|^2 e^{|q|t}(q/2\gamma - 1)/\gamma q$.

3. For nonzero damping in the $|qt_{\text{opt}}| \ll 1$ regime, the optimized diffusion gauge is

$$g''_{\text{opt}} \approx g_{\text{approx}} = \frac{1}{4} \log \left[\frac{(4\chi t_{\text{opt}} |n_0|)^2}{3} c_2(\gamma t_{\text{opt}}) + 1 \right], \tag{7.94a}$$

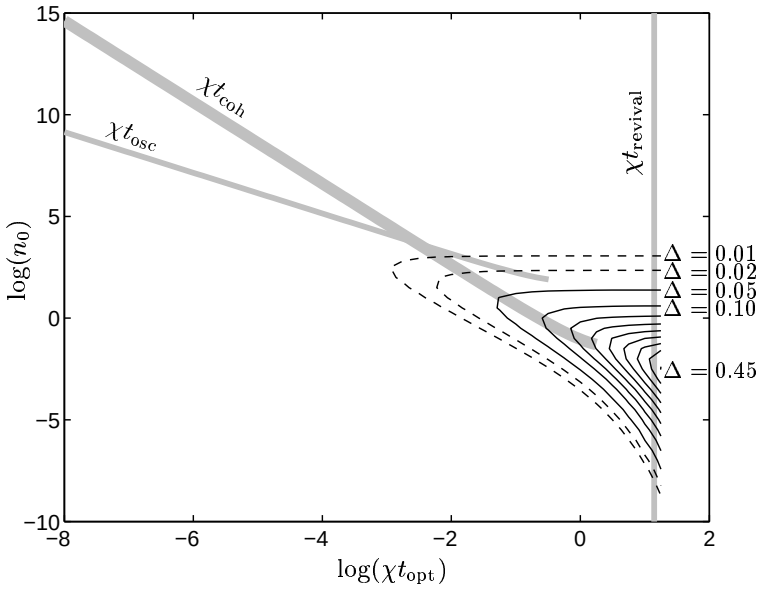

Figure 7.7: **Discrepancy** $\Delta = g''_{\rm opt} - g''_{\rm approx}$ between $g''_{\rm opt}$ (the exact optimization of g'' obtained by solving (7.52) using (7.92)) and the approximate expression (7.94). Displayed is the case of no damping ($\gamma = 0$) and classical initial occupation ($n_0 = n'_0$), shown as a function of $t_{\rm opt}$ and n_0. Discrepancy values Δ are shown as SOLID CONTOURS with spacing 0.05. Additional DASHED CONTOURS shown at very low discrepancy. For comparison, several physical timescales are also shown in GREY: time of first quantum revival $t_{\rm revival}$, phase coherence time $t_{\rm coh}$ and phase oscillation period $t_{\rm osc}$.

---

where the coefficient is

$$c_2(v) = \frac{3}{2}\left(\frac{e^{-2v}(3+2v)+1-4e^{-v}}{v^3}\right), \tag{7.94b}$$

which reduces to $c_2(0) = 1$ in the undamped case.

The discrepancy between (7.94) and the exact optimization obtained by solving (7.52) with (7.92) is shown for real n_0 for a wide range of parameters in Figure 7.7. It can be seen that for occupations $\gtrsim \mathcal{O}(10)$ and/or for times shorter than singly-occupied coherence time $1/2\chi$, the approximation is good. Compare with the analogous case with drift gauge shown in Figure 7.2.

For zero damping, and coherent state initial conditions $n_0 = n'_0$, and relatively short times $4\chi t e^{-2g''} \ll 1$ one finds

$$\mathrm{var}\,[G_L(t)] = \mathrm{var}[\widetilde{G}_L(t)] = \chi t \cosh 2g'' - 2(\chi t)^2 n'_0 + \frac{8}{3}\chi t (n'_0)^2 e^{-2g''}. \tag{7.95}$$

At large occupation n'_0, the gauge (7.94) gives $e^{g''} \approx (4\chi t_{\rm opt} n'_0)^2/3$, and one finds that all three terms in (7.95) are of similar size. Using the condition (7.43) the simulation time is

$$t_{\rm sim} \approx \mathcal{O}\,(10)\, t_{\rm coh}. \tag{7.96}$$

The $4\chi t e^{-2g''_{\rm approx}} \ll 1$ condition for $t < t_{\rm opt}$ implies large occupation $n'_0 \gg \mathcal{O}\,(1)$. At low occupation on the other hand, $e^{g''_{\rm approx}} \to 1$, the variances are $\approx e^{4\chi t} {n'_0}^2/4$, and one has again (7.82)

7.8.3 Numerical investigation of performance

The results of numerical simulations using such diffusion gauge only schemes are shown in Figures 7.8 and 7.9, in analogy with Figures 7.4 and 7.5 for the drift gauged schemes. Some data is also given in Tables 7.1 and 7.2. As before, simulations were made with $\mathcal{S} = 10^4$ for the mode occupations (7.87), and a wide range of target times $t_{\rm opt}$.

The four gauges simulated were all of the general form (7.94), but with the four adaptive varieties forms

$$g''(t) = g''_{\rm approx}(n_0, t_{\rm opt}) \tag{7.97a}$$

$$g''(t) = g''_{\rm approx}(n_0, t_{\rm rem}) \tag{7.97b}$$

$$g''(t) = g''_{\rm approx}(\breve{n}(t), t_{\rm opt}) \tag{7.97c}$$

$$g''(t) = g''_{\rm approx}(\breve{n}(t), t_{\rm rem}) \tag{7.97d}$$

in analogy with (7.75), where $t_{\rm rem}$ is given by (7.76). Otherwise, the procedure was the same as described in Section 7.7. Additional features beyond what is mentioned there include:

- The diffusion-gauge-only simulations give improvement over the positive P, but give simulation times $\mathcal{O}\,(4)$ times shorter than when combined with drift gauge (7.30). For example, compare Figure 7.8 to Figure 7.4). $t_{\rm sim}$ is still $\gg t_{\rm coh}$ at large n_0, however.

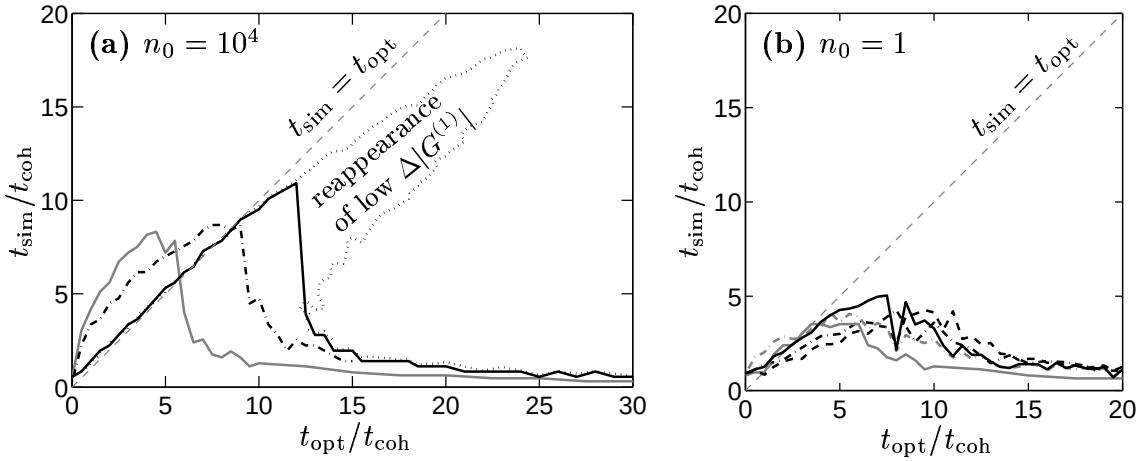

Figure 7.8: **Comparison of** *a priori* **target time** $t_{\rm opt}$ **with actual useful simulation time** $t_{\rm sim}$ for a variety of diffusion gauges in the $\mathcal{G} = 0$ schemes: Results for the four forms (7.97) are shown as: (7.97d) – SOLID DARK; (7.97c) – DASH-DOTTED LIGHT; (7.97b) – DASHED; (7.97a) – DASH-DOTTED DARK. Relationship obtained using the diffusion gauge (7.100) of Plimak *et al*[2] (but no drift gauge) is also shown (SOLID LIGHT). The dashed line in the background shows, for reference $t_{\rm opt} = t_{\rm sim}$. For the gauge (7.97d), the whole region where useful precision occurs is shown by the DOTTED line. Subplot **(a)**: mean particle number $n_0 = 10^4$, **(b)**: $n_0 = 1$.

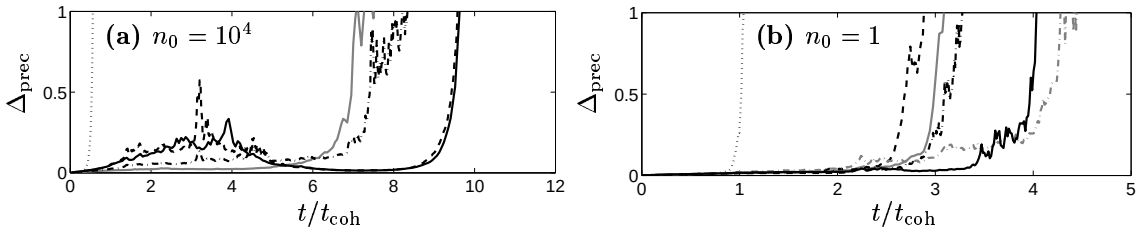

Figure 7.9: **Uncertainty in** $|G^{(1)}(0,t)|$, as a function of time for various $\mathcal{G} = 0$ schemes. The quantity plotted is $\Delta_{\rm prec} = \sqrt{\mathcal{S}/10^6}(10\ \Delta|G^{(1)}(0,t)|\,/\,|G^{(1)}(0,0)|)$, so that $\Delta_{\rm prec} \leq 1$ corresponds to useful precision as defined in Section 7.7.1. Results are plotted for the four diffusion gauge forms (7.97), shown as : (7.97d) – SOLID DARK; (7.97c) – DASH-DOTTED LIGHT; (7.97b) – DASHED; (7.97a) – DASH-DOTTED DARK. Data for the diffusion gauge (7.100) of Plimak *et al*[2] with $t_{\rm opt} = 3t_{\rm coh}$ (as used therein) is shown as a LIGHT SOLID line, while the ungauged positive P calculation is shown as a DOTTED line. Simulations were carried out with $\mathcal{S} = 10^4$ trajectories, starting with initial coherent state conditions: **(a)** $n_0 = 10^4$ **(b)** $n_0 = 1$. The diffusion-gauge plots in **(a)** were calculated with target times of $t_{\rm opt} = 10t_{\rm coh}$ for forms (7.97d) and (7.97b), and $t_{\rm opt} = 7t_{\rm coh}$ for forms (7.97c) and (7.97a). In subplot **(b)**, the four forms (7.97) were simulated with $t_{\rm opt} = 5t_{\rm coh}$.

- The full adaptive gauge form (7.97d) gives the most predictable results, in analogy to the drift-gauged case. That is, $t_{\rm sim} \approx t_{\rm opt}$ for times up till those given in Table 7.1.

- At low n_0' the simulation time appears more sensitive to the choice of $t_{\rm opt}$ than for the drift-gauged simulations.

- At high occupations $n_0' \gg 1$, the pairs of adaptive gauges (7.97d)&(7.97b) and (7.97a)&(7.97c) behave identically, and are thus not shown in all plots. The simulation appears to be insensitive to whether one uses a gauge choice dependent on $\breve{n}(t)$ or n_0. This is probably a feature peculiar to the particle number conserving single-mode anharmonic oscillator model, because here $\breve{n}(t) \approx n_0$ while useful precision is seen.

- For $n_0' \gg 1$, the time-adaptive gauge forms (7.97b) and (7.97d) lead to a peculiar effect if the optimization time $t_{\rm opt}$ is chosen larger than the usual maximum $t_{\rm sim}$ given in Table 7.1. The statistical error in the $G^{(1)}$ estimate first rises rapidly, then falls again, and finally grows definitively. This is seen in Figure 7.9**(a)**, and the parameter region for which this occurs is shown in Figure 7.8**(a)**. In effect one has two time intervals when the simulation gives useful results: at short times, and later in a time interval around $t \approx \mathcal{O}\left(10 t_{\rm coh}\right)$.

7.9 Comparison to recent related work

Improvements to the basic positive P simulation method for specific cases of interacting Bose gas systems have been tried with some success in several recent publications[1, 2, 3, 56]. Here we tie these together with the stochastic gauge formalism, and make some comparison to the results and analysis in the present chapter.

7.9.1 The work [1] of Carusotto, Castin, and Dalibard

The article *N-boson time-dependent problem: A reformulation with stochastic wavefunctions* considered an isolated (i.e. particle-conserving) system of $\overline{N}$ interacting

bosons. The "coherent state simple scheme" described in Section III B 2 therein can be identified as using drift gauges of the form

$$\mathcal{G}_{\mathbf{n}} = i\sqrt{2i\chi}\left(\alpha_{\mathbf{n}}\beta_{\mathbf{n}} - |\alpha_{\mathbf{n}}|^2\right) \tag{7.98a}$$

$$\widetilde{\mathcal{G}}_{\mathbf{n}} = \sqrt{2i\chi}\left(\alpha_{\mathbf{n}}\beta_{\mathbf{n}} - |\beta_{\mathbf{n}}|^2\right) \tag{7.98b}$$

when re-written in the notation of this thesis for a many-mode system as in equations (5.17), with mode labels $\mathbf{n}$. For the single-mode system considered in this chapter, this corresponds to

$$\mathcal{G}_1 = i\sqrt{2i\chi}\left(\breve{n} - |\alpha|^2\right) \tag{7.99a}$$

$$\mathcal{G}_2 = \sqrt{2i\chi}\left(\breve{n} - |\beta|^2\right). \tag{7.99b}$$

This gauge causes a full decoupling of the complementary α and β equations. Like (7.30) it is also successful in removing moving singularities, since the nonlinear terms in the radial equations for $d|\alpha|$ and $d|\beta|$ are removed.

There are two major differences between the coherent state wavefunction method and the gauge P method: Firstly, the former is hardwired to models that conserve particle number. This hardwiring to $\overline{N}$ particles has both a major benefit and a disadvantage, as compared to the gauge P method considered in this thesis:

- Benefit: coherent state amplitudes are not free to explore the entire phase space, are bounded from above, and cannot form moving singularities.

- Disadvantage: Losses or gains from external reservoirs are unable to be simulated, and so it is not applicable in its present form to simulations of e.g. evaporative cooling or a continuously loaded system such as an atom laser.

Another major difference is that diffusion gauges were not considered by Carusotto *et al*, and hence simulation times with this method for a single mode were very short ($\approx t_{\text{osc}}$).

The gauges (7.99) could also be applied to the present gauge P method, and their efficiency can be compared with the efficiency of gauges developed here: (7.30) when $g'' = 0$. The gauge (7.99) mediates the replacements $\breve{n} \to |\alpha|^2$ or $|\beta|^2$ in the $d\alpha$ and

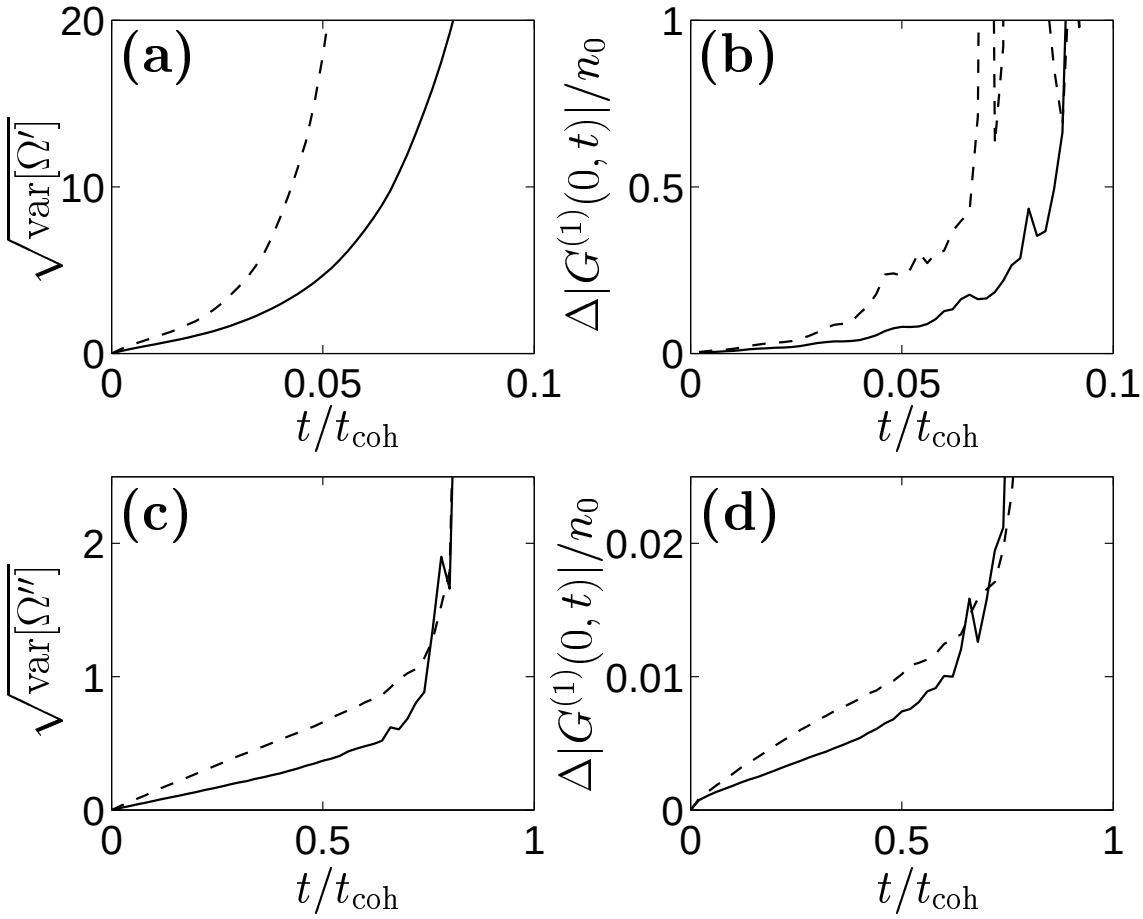

Figure 7.10: **Spread in trajectory weights** (**(a)** and **(c)**) *and phase correlation function uncertainties* (**(b)** and **(d)**), compared for the drift (only) gauges (7.99) – DASHED, and (7.30) (with no diffusion gauge: $g'' = 0$)– SOLID, in a one-mode, undamped, gainless system. Coherent state initial conditions with initial mean occupations **(a)** and **(b)**: $n_0 = 10^4$, while in **(c)** and **(d)**: $n_0 = 1$. All calculations are with 10^4 trajectories.

$d\beta$ equations (respectively), as opposed to (7.30), which only replaces $\breve{n} \to \mathrm{Re}\{\breve{n}\}$ and does not decouple $d\beta$ from $d\alpha$. So, since the magnitude of the spread in Ω behaves approximately proportional to $\sqrt{\sum_k |\mathcal{G}_k|^2}$, the gauge (7.99) is expected to produce a broader distribution of weights. Numerical simulations were carried out, and the results are shown in Figure 7.10 for both high and low mode occupations, , and Table 7.1 for high occupation. Useful simulation time with (7.99) is somewhat smaller than seen with (7.30).

In the same published work[1], a stochastic wavefunction method was developed based on Fock number states as well. This method was shown to give good results

and not be prone to boundary term errors but unfortunately does not appear extensible to open systems in any straightforward fashion because it is very strongly hardwired to $\overline{N}$ total particles.

The stochastic wavefunction method was also adapted in [1] to some cases of non-local interactions, arriving at equations that use effectively a similar noise expansion to that in (5.46), but were only applicable to potentials having exactly real Fourier transforms $\widetilde{U}_{\tilde{\mathbf{n}}} = \widetilde{U}'_{\tilde{\mathbf{n}}}$.

7.9.2 The work [2] of Plimak, Olsen, and Collett

The article *Optimization of the positive-P representation for the anharmonic oscillator* considered a single-mode undamped, gainless system at high Bose occupation with coherent state initial conditions. The "noise optimization" scheme applied therein to greatly improve simulation times can be identified as an imaginary diffusion gauge of the form (rewritten in the present notation)

$$g_{12} = \frac{i}{2}\cosh^{-1}\left[2n_0\chi t_{\rm opt}\right] = ig''_A \tag{7.100}$$

defined at high occupation or long times (i.e. while $2n_0\chi t_{\rm opt} \geq 1$). This is dependent on a target time $t_{\rm opt}$ (which was taken to be $t_{\rm opt} = 3t_{\rm coh}$ in the calculations of Ref. [2]), and the initial Bose occupation $n_0 = n'_0 = |\alpha_0|^2$. The value of the gauge was held constant throughout the calculation, without allowance for a changing mode occupation.

The useful simulation times obtainable with this method are also shown in Figures 7.3 and 7.5, and Table 7.1. Their precise dependence on the target time parameter $t_{\rm opt}$ has been calculated here, and is shown in Figure 7.4.

Comparing (7.100) with the optimized diffusion gauge (7.97a) that is constant with time, one finds that in the $n_0 \gg 1$ limit the two gauges differ by a constant:

$$g''_A(n_0, t_{\rm opt}) \approx g''_{\rm approx}(n_0, t_{\rm opt}) + \frac{\log 3}{4}. \tag{7.101}$$

While the simulation times achievable using g''_A are comparable with those obtained with the adaptive gauge $g''_{\rm approx}(\breve{n}(t), t_{\rm opt})$ of (7.97a), the target time $t_{\rm opt}$ is no longer

a good indicator, and has a complicated relationship with t_{sim}, as seen in Figure 7.8. The simulation time is also much shorter than with the drift gauged simulation.

Extensions to multi-mode systems or low mode occupations were not considered, however since the system under consideration was only a single mode, the lack of drift gauges did not lead to any boundary term errors in this particular case.

7.9.3 The work [3] of Deuar and Drummond

Some initial research by Drummond and Deuar into gauges for the single-mode undamped anharmonic oscillator system was reported in[3]. Here the state was written as an expansion over a normalized, Hermitian, coherent state projector kernel

$$\widehat{\Lambda}(\alpha,\beta,\theta) = \frac{e^{i\theta}||\alpha\rangle\langle\beta^*|| + e^{-i\theta}||\beta^*\rangle\langle\alpha||}{2e^{n'}\cos(\theta+n'')}, \tag{7.102}$$

where the phase variable θ was real. This is equivalent to imposing Hermiticity on the positive P kernel before normalizing it.

Drift gauges of the form

$$\mathcal{G}_1 = -\ \lambda\sqrt{\chi}\left[n''-n'+|\alpha|^2\right]\ [\tan(\theta+n'')+i] \tag{7.103a}$$

$$\mathcal{G}_2 = \ \lambda\sqrt{\chi}\left[n''+n'-|\beta|^2\right]\ [\tan(\theta+n'')+i] \tag{7.103b}$$

were used, where λ is a (real) strength parameter chosen *a priori*.

Simulation precision was greatly improved, but evident boundary term errors were present. This may have been caused by several factors, which are pointed out here because they are good examples of what should be avoided when choosing kernels and gauges:

1. The radial super-exponential behavior of $d\alpha$ and $d\beta$ is not removed in full, hence one can expect that moving singularities will still be present — as is ultimately seen as boundary term errors.

2. The magnitude of the kernel (7.102) diverges when $\theta \to -n''$. Hence, this parameter region might be unable to be sampled in an unbiased way. In particular, matrix elements of $\widehat{\Lambda}$ appearing in the expression (6.1) for $\widehat{\mathcal{B}}$ diverge when $\theta = \pm\pi/2$, and may lead to nonzero boundary terms once integrated.

3. The gauges were dependent on the trajectory weight $e^{i\theta}$, and thus non-autonomous. This causes feedback behavior between the phase-space variables α and β, and the weight, which is difficult to analyze to definitively determine whether moving singularities are present or not. (Compare to point 6(c) in Section 6.3.2).

4. The gauges diverge at $\theta \to \pm\pi/2$, against recommendation 6(b) of Section 6.3.2.

7.10 Gauge recommendation

Collecting together the analysis, and results of numerical calculations reported in this chapter, the following gauge choices appear to be advantageous for a single mode (labeled $\mathbf{n}$) of a two-body locally interacting Bose gas that is free to interact with its environment:

Defining

$$\breve{n}_{\mathbf{n}} = \alpha_{\mathbf{n}}\beta_{\mathbf{n}}, \tag{7.104}$$

then

$$\mathcal{G}_{\mathbf{n}} = -i\widetilde{\mathcal{G}}_{\mathbf{n}} = -\sqrt{2i\chi}\,\mathrm{Im}\left\{\breve{n}_{\mathbf{n}}\right\} e^{-g''_{\mathbf{n}}} \tag{7.105}$$

The local diffusion gauge dependent on the single "target time" parameter t_{opt}, or more precisely on the "remaining time to target"

$$t_{\mathrm{rem}} = \begin{cases} t_{\mathrm{opt}} - t \text{ if } t < t_{\mathrm{opt}} \\ 0 \quad \text{if } t \geq t_{\mathrm{opt}} \end{cases} . \tag{7.106}$$

is then given by

$$g''_{\mathbf{n}} = \frac{1}{6}\log\left\{8|\breve{n}_{\mathbf{n}}(t)|^2\chi t_{\mathrm{rem}} + a_2^{3/2}(\breve{n}_{\mathbf{n}}(t), \gamma_{\mathbf{n}}t_{\mathrm{rem}})\right\}, \tag{7.107}$$

i.e. (7.74). The coefficient a_2 is

$$a_2(\breve{n}, v) = 1 + 4\mathrm{Im}\left\{\breve{n}\right\}^2\left(\frac{1-e^{-2v}}{2v}\right) - 2|\breve{n}|^2\left(\frac{1-2v+2v^2-e^{-2v}}{v}\right). \tag{7.108}$$

7.11 Summary

The principal aim of this chapter has been to develop a "black box" form of drift and diffusion gauges. A form that can be expected to remove boundary term errors and extend simulation times beyond what is possible with the positive P for a single mode of a locally-interacting Bose gas with two-particle collisions that is open to the environment. The recommended form is given by (7.104)-(7.108). These gauges:

1. Extend simulation time for the anharmonic oscillator beyond what was possible with the positive P representation (i.e. when $g''_{jk} = 0$ and $\mathcal{G}_{\mathbf{n}} = \widetilde{\mathcal{G}}_{\mathbf{n}}$). For high mode occupations, the simulation time is extended by a factor of $\mathcal{O}\left(15n_0^{1/6}\right)$ (see Table 7.1) when starting from a coherent initial state, representative of a single trajectory. This simulation time is $\mathcal{O}(40)$ coherence times at high mode occupation, and all decoherence behavior is simulated. The improvement in numerical performance is best summarized by Figures 7.3, 7.6, and in Table 7.1.

2. Remove the instability responsible for moving singularities.

3. Apply for dynamically changing mode occupation.

4. Apply for simulations of open systems.

For the aim of using these gauges in many-mode simulations of open interacting Bose gases, it is crucial that the gauge choice be freely adaptable to any changes caused to the mode occupation (or other properties). Such changes will be caused by interactions with the rest of the modes, and an external environment.

A second possibly alternative method where only diffusion gauges are used has been considered, and appropriate optimized diffusion gauges derived. This method does not guarantee removal of systematic biases, but appears to have advantages in efficiency for many-mode calculations provided the simulation can be successfully monitored using the indicators of Gilchrist *et al*[64] to catch any boundary term errors if these form.

Lastly, the method developed has been tied in with and compared to some previous related work in the field[1, 2, 3].